EUROPEAN COMMISSION
5th EURATOM FRAMEWORK PROGRAMME 1998-2002
KEY ACTION : NUCLEAR FISSION

HTR-M

European Project for the development of HTR Technology - Materials for the HTR

CONTRACT N°
FIKI-CT-2000-00032
&
FIKI-CT-2001-00135

Materials for the Core and Internals: Synthesis of Materials Database

D. Buckthorpe, C.J. Earl

NNC

UK

Dissemination level : CO
Document Number: HTR-M-02/6-D-2.1.36
Deliverable 2.2

Materials for the Core and Internals: Synthesis of Materials Database (Control Rods)

by

D. E. Buckthorpe

&

C. J. Earl

C6463/TR/010
Issue 02
July 2004

DOCUMENT ISSUE RECORD
(engineering documents)

Adding value through knowledge

Document Title :	Materials for the Core and Internals: Synthesis of Materials Database (Control Rods)
Project Reference:	64631

Purpose of Issue : Final Issue

Security Class : Commercial-in-Confidence

Issue	Description of Amendment	Originator/ Author	Checker	Approver	Date
01	Initial issue	D. E. Buckthorpe C. J. Earl	M. Davies	T. Lennox	June 2002
02	Final Issue including comments from HTR-M partners	D. E. Buckthorpe C. J. Earl	M. Davies	T. Lennox	July 2004

Total number of pages:	Intro:	Text	Tables	Figures	Appendices
	vi	9	2	3	A21, B1,C3, D2, E5

Previous issues of this document shall be destroyed or marked **SUPERSEDED**

Distribution: S. Casalta, D.E.Buckthorpe, C.J. Earl, SINTER, HTR-TN, EDMS

3050aJan01 Controlling procedure - QP11, QP40 *Docprodref*

Table of Contents

List of Tables

List of Figures

Summary

This document contributes to the 5th Framework Project HTR-M, Work Package 2.1 and provides a summary of the results of a technical synthesis of the materials and the materials data for the internal structures of the High Temperature Reactor. As specified in the technical descriptions of the project the main aim is to review the materials and materials data for the control rod with particular emphasis on carbon-carbon (C/C) composites. The work summarises the results obtained during the first eighteen months of the HTR-M project and is seen as a first step in supporting the decisions made on selection of materials and test programme for the evaluation and testing phases of the work.

1. Introduction

This work contributes to the 5th Framework Project HTR-M, Work Package 2.1 and covers the results of a technical synthesis of materials and materials data for the core and internals of the High Temperature Reactor. As specified in the technical descriptions of the project the principle focus of this work item is on a review of materials and materials data for the control rod.

This document provides a summary of the results of a review of the materials and the materials data collected during the first eighteen months of the HTR-M project. This technical synthesis is seen as a first step in identifying a material or materials for study during the evaluation and testing phases of the HTR-M project

For the structural components at or near the highest gas temperatures, materials will be needed to resist the high thermal strains arising from power changes and load following requirements. Potential materials for such components, on current and test reactors, include AISI type 316 steel, Incoloy 800H (control rod) and Hastelloy XR. The former is normally used for components operating at temperatures up to 550-600°C and the last two for higher temperatures (750°C). These two have been extensively investigated for the HTTR.

For the database a limited number of materials has been chosen for the control rod. For this review the main emphasis has been placed on this component and in particular new materials such as carbon-carbon (C/C) composites. Metallic materials used for the control rod in existing reactor designs and test reactors have also been reviewed.

A summary of materials property data identified in the literature search has been collated and produced in table form in Appendix A. This and further data collected as the project progresses is to be transferred into the required format for inclusion into the overall project database.

2. Control Rod Designs & Material Considerations

The control rods are used to compensate for fuel burn-up and power variation reactivity effects. The control rods are positioned in the reflector and are used to control the reactor operation under normal operation modes and to shutdown the reactor system. Ref. 1 provides a synthesis of design use and specifications for the GTR-MH and PBMR listing the available information on loading conditions and environment.

For the HTTR control rod, these are individually supported by control rod drive mechanisms located in standpipes connected to the hemispherical top head of the reactor vessel. The neutron absorber in the control rods is made of B_4C/C and is sheathed with a cylindrical clad Incoloy 800H. In view of the temperature limitation of this alloy, the HTTR control rods are inserted in two steps to avoid damage by high temperature and heavy irradiation in the core. Nine out of the 16 pairs of control rods pairs are inserted first into the replaceable reflector column holes, while the other 7 pairs in the active core column holes are inserted 40 minutes later when the temperature of coolant at the outlet becomes lower than 750°C. Table 1 summarises the conditions in which the control rods operate in the HTTR reactor.

For several years, JAERI have been performing tests on C/C composites as potential alternatives to Incoloy 800H for the control rod material. The design of such a control rod made with carbon-carbon composite material consists of a series of separate segments joined together to form a single rod. Each segment contains an absorber material (usually in the form of sintered rings of B_4C) located between two coaxial tubes. Figure 1 shows the segmented arrangement proposed for the HTTR Reactor using C/C composite material. Such a development is underway in order to avoid the two stage trip insertion necessary with the 800H sheath material. The HTTR control rod consists of an outer and inner sheath tube, bolts and joints, which are all made of three dimensional C/C composite material. New three dimensional carbon fibre weaving techniques were applied in the manufacture. In particular, the rod is strengthened in circumferential, radial and axial directions with a high content of carbon fibres, and the matrix material is filled with a specific process to achieve a high density.

3. Materials Requirements

The materials for the control rod are required to be stable at very high temperatures. A first attempt to clarify the material property and test requirement was made (Ref. 2) based on a review of the R&D work performed at JAERI. Temperatures of the order of 1000°C should be achievable to allow the reactor core to operate with an increased margin of safety. Also there is a need for stable fracture behaviour. In a recent paper, JAERI has summarized the data requirements for the design of the control rods made for C/C composites (Table 2).

Other important properties include thermal conductivity, thermal diffusivity, dimensional change and Young’s Modulus. Neutron irradiation has a severe degradation effect on carbon based materials such as graphite and C/C composites and knowledge of their properties under neutron irradiated conditions is required.

4. Candidate Materials and Properties

The main emphasis has been placed on C/C composites and Incoloy 800H for the control rod. Incoloy 800H is selected because it has been chosen as the cladding material for the neutron absorber rods for the HTTR.

The C/C composites considered in the technical survey are listed in Table 3 along with reference and information on the supplier where available.

The following sections summarise the information collected to date for these materials.

4.1 Incoloy 800H

Design properties for non-irradiated 800H are given in design codes such as ASME section NF. These contain allowable stresses and design fatigue curves up to 750°C. Such properties are suitable for applications where environmental effects are negligible.

For the control rod, the property information is needed in the post-irradiated condition and in a helium atmosphere. A number of published papers deal with the derivation of properties in heat exchanger applications, and when used in HTGR atmospheres. Some results are given in Ref. 18 in helium and air and at temperatures of 900°C. Ref. 21 reports on results in air and helium at temperatures of 950^{o}C suggesting significant changes in fatigue behaviour between the two environments.

Appendix D lists the references located that provide property information in helium. The documents are also given as references 17-22 in section 7. A table of property values taken from these references is given in Appendix B. These cover graphical results for fatigue and creep-fatigue behaviour up to 1000^{o}C. Contamination of the helium with impurities such as H_2, H_2O, CH_4, CO and CO_2 can lead to oxidation and carburisation. Carburisation can lead to a significant reduction in creep strength. Ref. 19 examines the effect of different environments on carburisation and showed the importance of controlling of the oxygen potential of the service environment.

Loss of creep ductility due to irradiation induced damage in helium is an important property. From the papers reviewed on this material (ref.18- see Appendix E) no published information was found with respect to post-irradiated properties.

4.2 Carbon-Carbon Composites

Low doses of neutron irradiation at temperatures below 600^{o}C can cause a significant decrease in properties of practically all the carbon based materials. Irradiation of fast neutrons causes displacement of carbon atoms from the lattice into interstitial locations. This leaves vacancies in the basal plane of the material. As the temperature increases, the mobility of the interstitial carbon atoms increases, and eventually these join to form new clusters or planes. The vacancies also become mobile at high temperature and can cluster and collapse. Irradiation induced damage has been shown to cause significant changes in thermal conductivity, dimension change, thermal expansion (CTE) and strength.

The structure of C/C composite materials is an-isotropic, and dimensional changes are very dependent on axis direction. At low neutron fluences radiation induced shrinkage is mainly within the graphite planes (axial and azimuthal directions on the fibre) with swelling in the other direction accomodated by pores or voids. At higher fluences these materials undergo “turnround” when the rate of shrinkage slows and stops and the material begins to re-expand. The exact form of the dimensional change curve varies with irradiation temperatures. Generally, the higher the temperature the lower the peak shrinkage and the lower the dose at which turnaround occurs. Different C/C composites can have significantly different dimensional change curves at the same temperatures.

The information available for C/C composites is very specific and much less than for metals. Some information is available in the non-irradiated condition but for this application irradiated properties are most important. The following sections summarise the results obtained from a review of documents available from R&D for HTR and Fusion applications.

4.2.1. Thermal Conductivity

Thermal conductivity is an important physical property for control rod materials. The thermal conductivity of these materials can be the order of 700 W/m K at room temperature, before irradiation. This value reduces sharply however with increasing temperature. Composites that have the highest room temperature value often experience the sharpest reduction at high temperatures. It is generally found that although the relative temperature reduction and final value are dependent on the particular composite, the differences between them are greatly reduced at high temperature (Fig. 2).

For C/C composites as with all carbon based materials (i.e. graphites), the thermal conductivity is severely degraded by neutron irradiation. The level of degradation is dependent on irradiation condition and temperature. For C/C composites neutron induced degradation can occur at fluxes as low as 10^{-3} dpa and irradiation temperatures of 200-600^{o}C (Refs. 3, 6). Ref. 3 considers the effect of irradiation on thermal conductivity for CX2002U a felt type C/C composite CX2002U manufactured by Toyo Tanso. A marked reduction in conductivity is shown in comparison to the non-irradiated value (Fig. 2). The reduction is greatest at room temperature and the level of degradation decreases with increasing temperature.

Refs. 11 and 12 compare two three-dimensional C/C composite materials (223 PAN fibre and 222 pitch fibre). Results have been reproduced in figure 1 for the non-irradiated, irradiated and irradiated plus annealed (to 1600^{o}C) conditions parallel to the fibres. At the temperature of the irradiation, the reduction is approximately 50-60% of the non-irradiated value with little change between 1.5 and 4.0 dpa. The effect of thermal annealing afterwards is to recover the values to within 20-30% of the non-irradiated levels.

For much smaller doses Ref. 6 presents normalised conductivity values for three C/C composites at different neutron dose levels (between 10^{-3} and 10^{-1} dpa) and irradiation temperatures (400 and 600^{o}C). At 0.1 dpa (10^{24} n/m^{2}) the thermal conductivity of a carbon fibre composite (CFC) called A05 (Carbonne Lorraine) decreased by ~45% (T_{irr} = 400^{o}C) and ~30% (T_{irr} = 600^{o}C). At 10^{-3} dpa the reduction was <10% at both temperatures and < 20 to 30% at 10^{-2} dpa. Annealing at a temperature of 2100^{o}C for 30 minutes effectively recovers the initial thermal conductivity.

Figure 2 collates published results for thermal conductivity changes with temperature and irradiation conditions for a range of C/C composites. The general conclusion was that C/C composite materials irradiated under the same conditions had practically the same value and same temperature dependence of conductivity irrespective of the original non-irradiated conductivity values.

4.2.2 Thermal Diffusivity

This is an important physical property with respect to the thermal shock resistance of the material. Measurements have been made using the Laser Flash method (Ref. 4) for two C/C composite materials 190G and A05. The specimens were irradiated in the JMTR to a maximum fluence of 1.98 x 10^{25} n/m^{2} (approx. 1.3 dpa) at temperatures between 640-1070^{o}C. For A05 the diffusivity at the highest fluence was reduced to around 30% of its non-irradiated value at 20^{o}C and around 50% of its non irradiated value at 600-800^{o}C. For 190G the difference was similar at higher temperatures but more pronounced at room temperature. Figure 3 compares the two materials. Also included are values reported in Ref. 6 for A05.

Ref. 8 presents results for three different C/C composite materials before and after irradiation. For two C/C composites (designated A & B) irradiated at a total neutron fluence of 1.2 x 10^{25} n/m^{2} and irradiation temperature 750~850^{o}C a reduction in thermal diffusivity to 80% of the non-irradiated value was obtained. For a 2D C/C irradiated with a total fluence of 1.75~1.8 x 10^{25} n/m^{2} and 650~710^{o}C irradiation temperature the thermal diffusivity reduced to 53% of the non-irradiated value. These values have also been introduced on to Figure 2 for comparison.

4.2.3. Density

Mean bulk density values for irradiated and non-irradiated specimens are given in Ref. 6 for three C/C composites irradiated at fluences between 1.2 & 1.75~1.88 x 10^{25} n/m^2 and irradiation temperatures between 650~850^{o}C. The effect of irradiation damage is to increase density values by between 1 and 5%. For A05 irradiated at 0.1 dpa the results in Ref. 4 show a variation with temperature (up to 400^{o}C & 600^{o}C respectively) between 1.812 and 1.808 for a sample with T_{irr} = 400^{o}C and 1.799 to 1.791 for T_{irr} = 600^{o}C. Overall bulk density values for the range of C/C composites were in the range of 1.5 to 1.8 g/cm^3.

4.2.4. Specific Heat

Non-irradiated manufacturers values for specific heat are given in Ref. 8 for five C/C composite materials. These range form 0.7 to 0.76 J/gK. No irradiated material data was found.

4.2.5 Coefficient of Thermal Expansion (CTE)

From the papers studied only non-irradiated properties of thermal expansivity or expansion coefficient were found and only typical or manufacturers values quoted. The level of anisotropy in some cases however was quite marked (e.g. from Ref. 7, CC 312: 0.6 (¦), 10.9(⊥) x 10^6/^{o}C).

4.2.6 Dimensional change

Dimensional change is an important property in carbon-based materials. The most notable effect occurs in graphites where the same material can experience both a contraction and an expansion due to irradiation damage, depending on the level of neutron flux it's exposed to. In explanations of such behaviour in graphites the term frequently used it "turnround". For C/C composites the dimensional change property has been investigated in Ref. 12 for three different materials irradiated at 600^{o}C (see Fig.4). A unidirectional 1-D C/C composite showed a very an-isotropic dimensional change. There was rapid shrinkage initially in the fibre direction plus, in the direction perpendicular to the fibres (diameter), there was shrinkage up to a fluence of 1 dpa, followed by a reversal to expansion reaching the original diameter at about 2.5 dpa. Above 2.5 dpa the diameter continued to expand at an increasing rate. For a 2-D composite the "turnround" was seen in both directions although the effect was much less. For the 3-D composite isotropic behaviour was seen at fluences up to 2 dpa whereas for greater doses, the composite x direction continued to show shrinkage, and the fibre x-y (diameter) direction a reversal and slight growth. Comparison of dimensional change of pitch (FM1-222) and PAN (FM1-223) fibre composites in the z-fibre direction showed the pitch fibre composite to be superior.

Results in Ref. 9 for composites irradiated up to around 2 x 10^{25} n/m^2 a pitch C/C composite MCI showed expansion (up to 3%) in the y direction and contraction (to 2%) in the x-direction. For CX2002U contraction was seen in both directions, up to around 1.8% in the y-direction and <0.5% in the x-direction.

Data in Ref. 6 and Ref. 15 report on irradiation induced swelling in 2-D and pseudo 3-D composites of the order of ~20% under high neutron damage of 5dpa. The latter also notes the tritium retention potential of the material which may also have to be considered.

4.2.7 Young's Modulus

The Young's Modulus of the material is an important indicator of elastic strength. Irradiated (2 x 10^{25} n/m^2) and non-irradiated values for three different C/C composites are given in Ref. 7. An increase in Young's Modulus was found for MFC (23%) and CX2002U (6%), with the effect most pronounced in the direction parallel to the fibres. For CC-312 a reduction (~8%) was observed. In Ref. 9 increases in Young's Modulus of over 30-40% are recorded with the most pronounced effect shown at low doses for MCI composite (0.6 x 10^{25} n/m^2) of around 100%. Also for CC-312 an increase (approx. 10%) was observed at low dose and a slight reduction (<3%) at the higher dose (2 x 10^{25} n/m^2). Ref. 8 gives values before and after irradiation for three C/C composites. For C/C-A and B, exposed to a neutron fluence of 1.2 x 10^{25} n/m^2 increases of 42% and 30% were observed. For a 2-D C/C composite exposed to 1.75~1.88 x 10^{25} n/m^2 the increase was 33%.

4.2.8 Bending Strength

A comparison is made in Ref. 7 between irradiated and non-irradiated values of three C/C composite materials. The failure strain for un-irradiated CC-312 bending strength of MFC-1 decreased after irradiation. For CC-312 & CX2002U the strength increased and bending fracture strain to decrease after irradiation.

5. Discussion

The operational experience with HTTR has shown shortcomings with respect to the use of Incoloy 800H for the control rod material. For several years JAERI have been investigating alternatives that allow the component to reach higher temperatures without suffering damage. Such materials include AC250 (Across Ltd.) and CX-270 (Toyo Tanso) characterised using measurements of mechanical and physical properties. The materials were in the form of tubes and bolts.

The findings of the JAERI work and of other authors confirms that properties of the C/C composites are largely an-isotropic. Also for C/C composites as with all carbon based materials (i.e. graphites), property values can be severely degraded by neutron irradiation, the level of degradation being dependent on irradiation condition and temperature.

From the references studied some irradiation induced properties were available for C/C composites for thermal conductivity, thermal resistivity and dimensional change. These are presented in graphical form in the report. Other properties for which some irradiation data has been published includes bending strength, Young's Modulus and density. Only non-irradiated data was available for the CTE and specific heat.

Some general trends in behaviour can be seen in properties such as thermal conductivity and thermal resistivity, each showing marked changes due to the effects of irradiation and temperature. A trend curve on thermal conductivity vs dpa level at 150^{o}C is shown in figure 5 taken from Ref. 15. It should be realised however that different materials can show different absolute values and in some cases improvements in thermal properties can be at the expense of other important property values. Care must therefore be exercised if using such trend curves and if using a combination of properties from different composites to estimate potential properties of new materials.

6. Conclusions & Recommendations

This document provides an initial review and a first step towards identifying the types of materials that can be used for control rods of future HTRs.

Experience with HTTR has shown shortcomings with respect to the use of Incoloy 800H material. A two-stage reactor trip sequence is used to avoid high temperatures and high irradiation damage in the material. Use of a C/C composite material that resists much higher temperatures is under investigation by JAERI. The use of such materials will produce an increase in the thermal resistance of the control rod enabling the reactivity control to be less restrictive during shutdown. It also has a potential in allowing the normal operating temperatures of future reactors to be increased.

For a control rod made from a C/C composite materials the validation of through life performance is critically dependent on the knowledge of the composite material properties. These are irradiation dependent. It is essential that material behaviour is fully understood and investigated. Information has been assembled for a range of different composite materials (i.e. thermal conductivity, thermal resistivity, dimensional change, etc.). The database of properties on C/C composites being compiled will provide a basic platform of data that can be used to support such investigations.

Some trends in behaviour have been observed with respect to thermal conductivity and thermal resistivity against temperature and irradiation damage.

In choosing a candidate material it is important to assess whether all the design requirements can be met and to list the material property requirements in priority order. Care must be exercised if using a combination of properties from different composites as any one material can have some highly favoured properties but at the expense of others, e.g. N3M composites will exhibit low radiation swellling but at the expense of lower thermal conductivity.

7. References

Ref

1 B. Riou
HTR-M Design use and specification for internals
HTR-M Report HTR-M 01/07 D 2 1 14

2 R. Couturier
HTR-M WP2, Milestone 2 Materials review and database
HTR-M Report HTR-M 01/09 D 2 0 12

3 T. Maruyama and M. Harayama
"Neutron Irradiation effect on the thermal conductivity and dimensional change of graphite materials"
Journal of Nuclear Materials 195 (1992), North-Holland, pp 44 - 50

4 H. Matsuo and T. Nagasaki
"Thermal diffusivity of neutron irradiated carbon-carbon composites"
Journal of Nuclear Materials 217 (1994), pp 300 - 303

5 F. Gao, J. W. Patrick and A. Walker
"The characterisation of cracks and voids in two dimensional carbon-carbon composites"
Loughborough University of Technology (1992), pp 103 - 108

6 C. H. Wu, J. P. Bonal and B. Thiele
"Thermal conductivity changes in graphites and carbon/carbon fibre materials induced by low neutron damages"
Journal of Nuclear Materials 212-215 (1994), pp 1168-1176

7 M. Eto, S. Ishiyama, H. Ugachi, K. Fukaya and S. Baba
"Mechanical properties of neutron irradiated carbon-carbon composites for plasma facing components"
Journal of Nuclear Materials 212-215 (1994), pp 1223 - 1227

8 S. Sato, A. Kurumada, K. Kawamata, R. Ishida, T. Takizawa and Teruyama
"Evaluation of Performance for Plasma Disruption and Neutron Irradiation for graphites and C/C Composites for First Wall Components for Fusion Reactor Devices"
Journal - Atomic Energy Society of Japan Vol. 32 (1990), pp 1124 - 1132

9 H. Ugachi, T. Oku, S. Ishiyama and M. Eto
"Effect of Irradiation on Mechanical Properties of Carbon Composite Materials"
Transactions - Japan Society of Mechanical Engineers Series A vol. 62 A (1996), pp 10-17

10 T. D. Burchell, W. P. Eatherly and G. E. Nelson
"Radiation Damage in Carbon-Carbon Composites"
Carbon - 5th international conference (1992), pp 985 – 986

11 T. D. Burchell, W. P. Eatherly and J. P. Strizak
"The Effect of Neutron Irradiation on the Structure and Properties of Carbon-Carbon Composite Materials"
Effects of Radiation on Materials: 16th International Symposium, ASTM STP 1175 (1993), pp 1266 - 1282

12 T. D. Burchell
"Irradiation induced structure and property changes in Tokamak plasma facing C/C composites"
39th International SAMPE Symposium April 11-14 (1994), pp 2423 - 2436

Ref

13 M. Roedig, W. Baur and B. Woscheck
"Burst Tests to Measure the Tangential Strength of CFC Tubes"
The Status of Graphite Development for Gas Cooled Reactors. Proceedings of a Specialists Meeting held in Tokai-Mura, Japan, 9-12 September 1991, pp 59 - 63

14 M. Eto, S. Iishiyama, K Fukaya, T. Saito, M. Ishihara and S. Hanawa
"Development of Carbon/Carbon Composite Control Rod for HTTR (II) - concept, specifications and mechanical test of materials"
Japan Atomic Energy Research Institute (1998)

15 T. Munsat
"High Temperature Carbon-Irradiation Issues for the Sombrero ICF Reactor"
Prinston Plasma Physics Laboratory, Sept 1999

16 M. Eto, T. Arai, T Konishi
The fatigue strength of graphite and carbon materials for HTTR core components
Japan Atomic Energy Research Institute (1998)

17 H. Nickel, F. Schubert and H. Schuster
"Evaluation of Alloys for Advanced High-Temperature Reactor Systems"
Elsevier Science Publishers B.V. (North Holland Physics Publishing Division) (1983), pp 251 - 265

18 E. Bodmann, H. Diehl, I. Blume-Firla and H Demus
"Service Conditions and Relevant Properties of HTGR Materials"
Proceedings of a specialists meeting organised by the International Atomic Energy Agency, held in Cracow, 20-23 June 1988 pp 15 - 27

19 H. Tsuji, H. Nakajima and T. Kondo
"Current Status of Studies on High Temperature Metallic Materials for HTGR Applications in JAERI"
Proceedings of a specialists meeting organised by the International Atomic Energy Agency, held in Cracow, 20-23 June 1988, pp 81 - 90

20 W. R. Johnson and G. Y. Lai
"Interaction of Metals with Primary Coolant Impurities: Comparison of Steam-Cycle and Advanced HTGRs"
Specialists Meeting on High Temperature Metallic Materials for Application in Gas-Cooled Reactors Vienna, Austria 4-6 May 1981, pp J1 – J22

21 H. Inouye and P. L. Rittenhouse
"Relationship Between Carburisation and Zero-Applied-Stress Creep Dilation in Alloy 800H and Hastelloy X"
Specialists Meeting on High Temperature Metallic Materials for Application in Gas-Cooled Reactors Vienna, Austria 4-6 May 1981, pp L1 – L12

22 H. P. Meurer, H. Breitling and E. D. Grosser
"Fatigue and Creep Fatigue Behaviour of High Temperature Alloys for HTR Application"
Specialists' Meeting on High Temperature Metallic Materials for Application in Gas-Cooled Reactors Vienna, Austria 4-6 May 1981,pp U1 – U12

Table 1 Service conditions for the HTTR control rods.

	Maximum temperature (℃) (Bottom of the lowest sleeve)		Fluence (660 days***) (Bottom of the lowest sleeve)
	Normal operation (950℃) (Location : B+0.75 level)	Scram (Loss of commecial electricity)	
Central control rod	~610*	~1050** (One-step insertion) ~800* (Two-step insertion)	$\sim 6\times10^{24}$ n/m^2
R2 control rod	~560*	~900*	$\sim 6\times10^{24}$ n/m^2

* : Systematic and random factors conidered.
** : Temperature of control rod guide block.
*** : Lifetime of the control rod is about 5 years (depends of creep property).
B : Top of the core.

Table 2 Summary of material testing and database requirements for the design of the control rods (JAERI)

Test item	Properties	Database
Strength test Fatigue test	Static strength, Fracture strain, Strength distribution, Fatigue strength, Effect of environment and irradiation	Design stress strength, Design yield stress, Design tensile strength, Poisson's ratio, Longitudinal elastic modulus, Allowable fatigue life
Creep test	Creep strength, Creep fatigue	Design creep fracture strength
Thermal expansion		Thermal expansion coefficient
Thermal conductivity		Thermal conductivity

Table 3 Carbon-carbon composites considered in the technical survey

Material	**Reference**	**Type**	**Supplier**
190 G	4		Not given
222	10, 11		Fiber Materials Inc.
223	10, 11, 12		Fiber Materials Inc.
2D-C/C	8	Rayon carbon fibre	Not mentioned
AC 250	14		Across Co.
A05	4, 6, 10, 11		Le Carbonne Lorraine
C/C-A	8	Pitch carbon fibre	Showa Deniko
C/C -B	8	PAN, carbon fibre	Showa Deniko
CC 2001 G	13		SIGRI
CX 270	14		Toyo Tanso
CX-2002U	3, 7, 8, 9	PAN, carbon fibre	Toyo Tanso
DMS 678	6		Dunlop
FMI 4D	6		Fiber Materials Inc.
MCI	9		Not given
MFC-1	7		Mitsubishi Chemical Industries
PCC-1S	8	PAN, carbon fibre	Hitachi Chemical
RFC	10, 11, 12		Fiber Materials Inc.
UFC	10, 11, 12		Fiber Materials Inc.

Figure 1 Segmented Control Rod Arrangement used on the HTTR

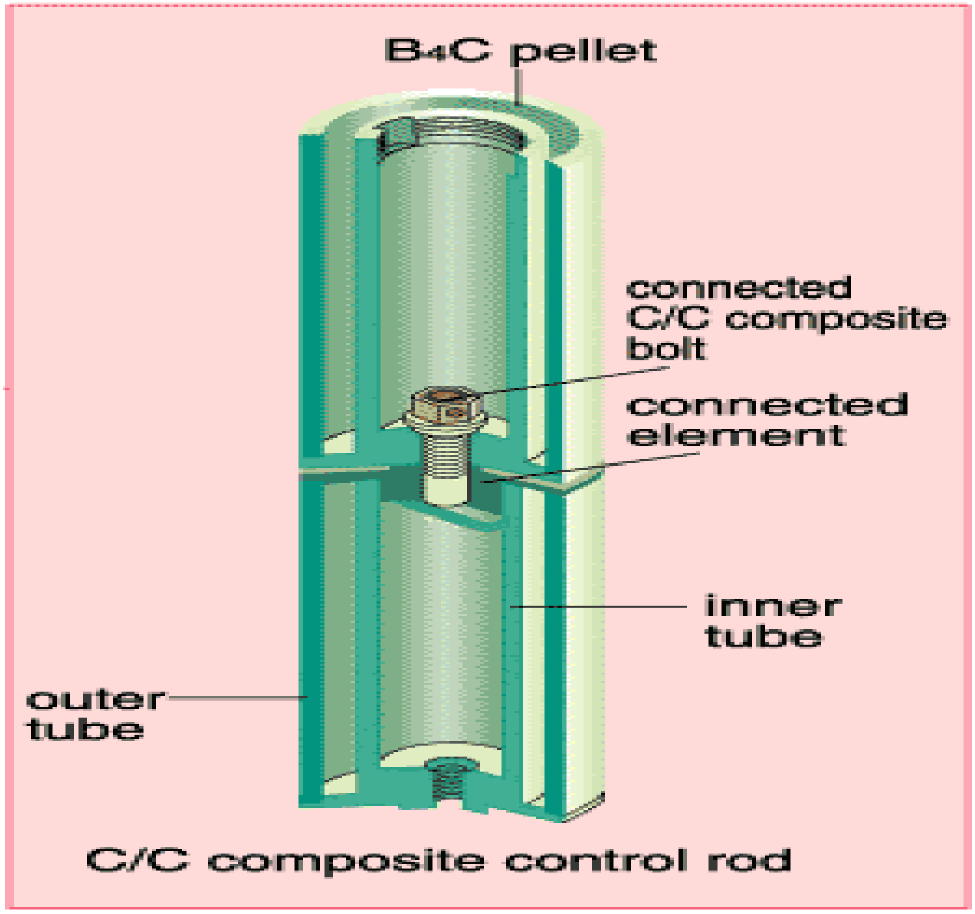

Figure 2 Thermal Conductivity Changes with Temperature and Irradiation Conditions

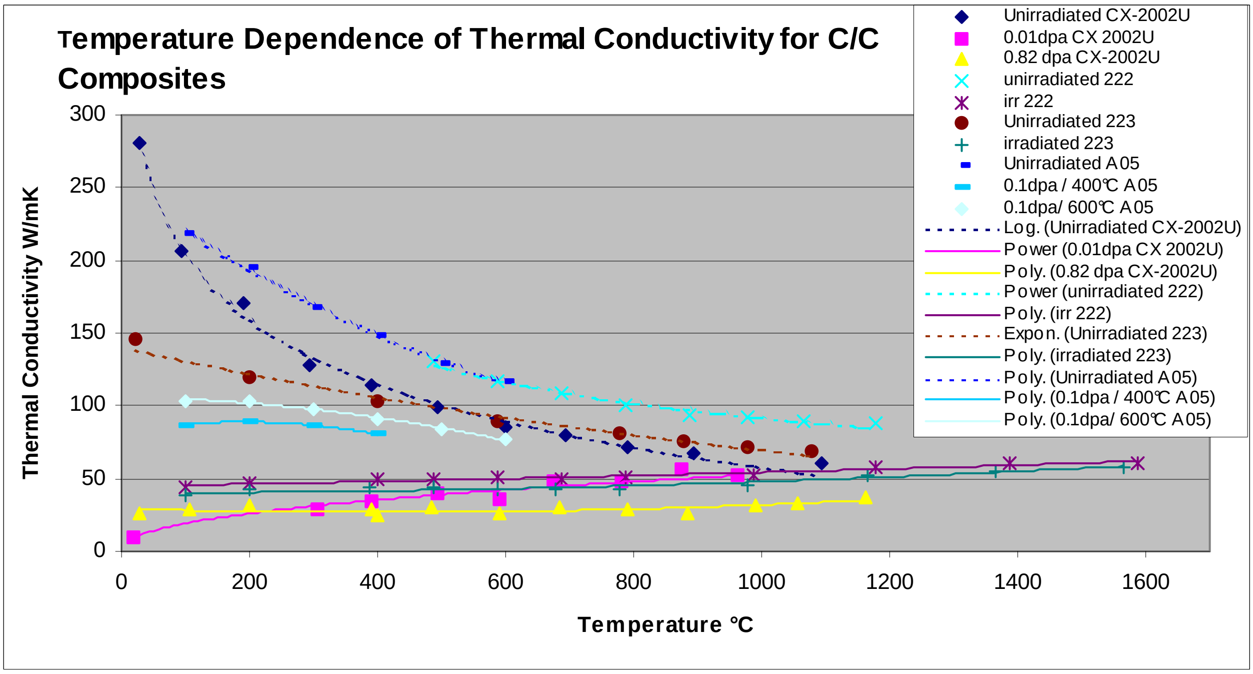

Figure 3 Thermal Diffusivity Changes with Temperature and Irradiation Conditions

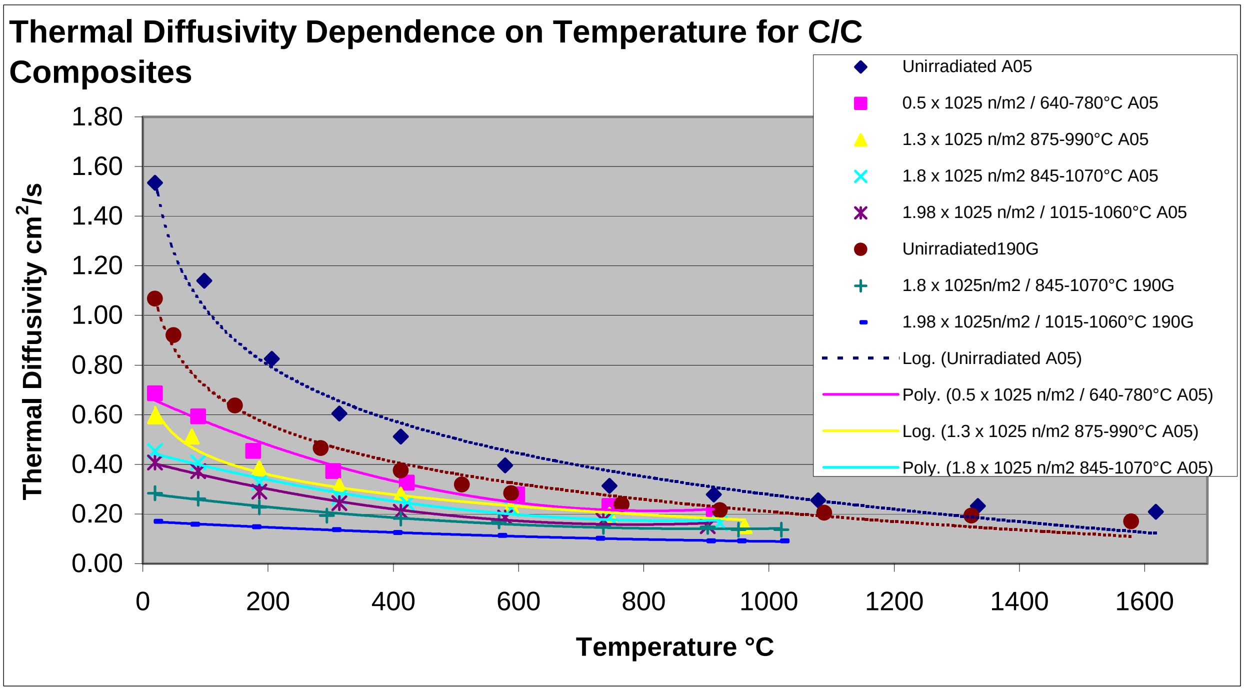

Figure 4 Dimensional Changes

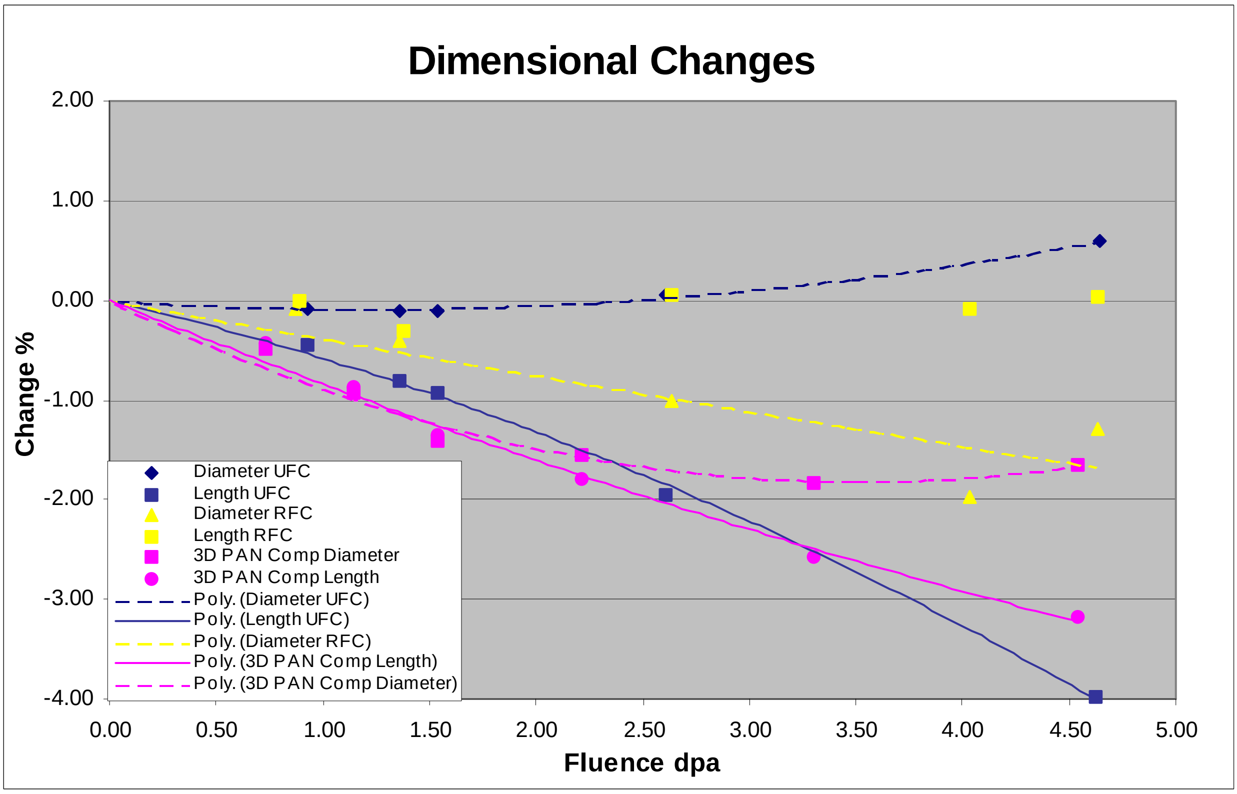

Figure 5 Normalised Conductivity verses damage level

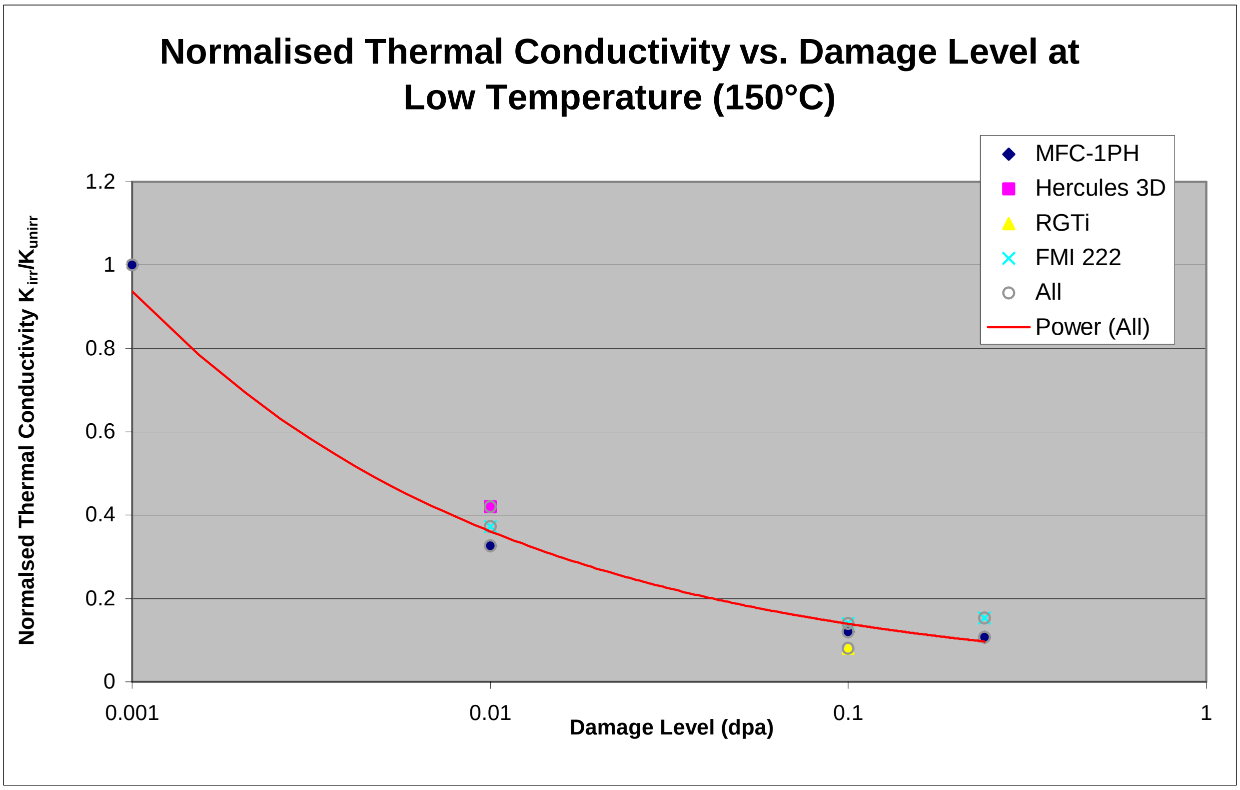

Appendix A: Carbon/Carbon Composite Information Tables

A1 190G

Mechanical Property	Value	Units	Reference	Notes
Thermal diffusivity (g)			4, Fig 3, Page 301	Graph shows the radiation induced changes in thermal diffusivity of the material 190G (JMTR 1.98 x 10^{25} n/m^2, 640-1070°C E > 29 fJ)
			4, Fig 5, Page 302	Graph shows the changes in temperature dependence of normalised thermal diffusivity of the material 190G (JMTR 1.98 x 10^{25} n/m^2, 640 - 1070°C E > 29 fJ)

A2 222

Mechanical Property	Value	Units	Reference	Notes
Diameter Change			10, Fig 5, Page 987	Graph shows the radiation induced diameter changes in 222 (2.44 x 10^{25} n/m^2, E > 50 keV, 1.6 dpa or 7.28 x 10^{25} n/m^2, E > 50keV, 4.7dpa)
Diameter Change			11, Fig 7, Page 1274	Graph shows the radiation induced diameter changes in 222 (2.44 x 10^{25} n/m^2, E > 50 keV, 1.6 dpa or 7.28 x 10^{25} n/m^2, E > 50keV, 4.7dpa)
Dimensional Changes			12, Fig 8 (a) & (b), Page 2434	Graphs show the irradiation induced dimensional changes 222 (2.44 x 10^{25} n/m^2, E > 50 keV, 1.6 dpa or 7.28 x 10^{25} n/m^2, E > 50keV, 4.7dpa)
Fractional Change in Strength	1.00		11, Table 2, Page 1276	Unirradiated at 2650°C
	1.39		11, Table 2, Page 1276	Irradiated at 2650°C a fluence of 0.6 DPA - E > 50keV
	1.33		11, Table 2, Page 1276	Irradiated at 2650°C a fluence of 0.85 DPA - E > 50keV
	1.62		11, Table 2, Page 1276	Irradiated at 2650°C a fluence of 1.78 DPA - E > 50keV
	1.00		11, Table 2, Page 1276	Unirradiated at 3100°C
	1.33		11, Table 2, Page 1276	Irradiated at 3100°C a fluence of 0.68 DPA - E > 50keV
	1.64		11, Table 2, Page 1276	Irradiated at 3100°C a fluence of 2.01 DPA - E > 50keV
Fracture Strength	59.7± 12.0	MPa	11, Table 2, Page 1276	Unirradiated at 2650°C
	82.9	MPa	11, Table 2, Page 1276	Irradiated at 2650°C a fluence of 0.6 DPA - E > 50keV
	79.4	MPa	11, Table 2, Page 1276	Irradiated at 2650°C a fluence of 0.85 DPA - E > 50keV
	96.6	MPa	11, Table 2, Page 1276	Irradiated at 2650°C a fluence of 1.78 DPA - E > 50keV
	49.3 ± 0.5	MPa	11, Table 2, Page 1276	Unirradiated at 3100°C

Mechanical Property	Value	Units	Reference	Notes
	65.8	MPa	11, Table 2, Page 1276	Irradiated at 3100°C a fluence of 0.68 DPA - E > 50keV
	80.8	MPa	11, Table 2, Page 1276	Irradiated at 3100°C a fluence of 2.01 DPA - E > 50keV
Length Change			10, Fig 4, Page 987	Graph shows the radiation induced length changes in 222 (2.44 x 10^{25} n/m^2, E > 50 keV, 1.6 dpa or 7.28 x 10^{25} n/m^2, E > 50keV, 4.7dpa)
Length Change			11, Fig 6, Page 1274	Graph shows the radiation induced length changes in 222 (2.44 x 10^{25} n/m^2, E > 50 keV, 1.6 dpa or 7.28 x 10^{25} n/m^2, E > 50keV, 4.7dpa)
Strength			11, Fig 9, Page 1277	Graph shows the effect of neutron irradiation on the strength of 222 (2.44 x 10^{25} n/m^2, E > 50 keV, 1.6 dpa or 7.28 x 10^{25} n/m^2, E > 50keV, 4.7dpa)
Thermal Conductivity			11, Fig 11, Page 1279	Graph shows the effect of temperature on thermal conductivity for 222 (2.44 x 10^{25} n/m^2, E > 50 keV, 1.6 dpa or 7.28 x 10^{25} n/m^2, E > 50keV, 4.7dpa)
			11, Fig 12, Page 1280	Graph shows the effect of post-irradiation annealing on the thermal conductivity of 222 (2.44 x 10^{25} n/m^2, E > 50 keV, 1.6 dpa or 7.28 x 10^{25} n/m^2, E > 50keV, 4.7dpa)
Thermal Conductivity			12, Fig 10, Page 2435	Graph shows the temperature dependence on thermal conductivity for 222 (2.44 x 10^{25} n/m^2, E > 50 keV, 1.6 dpa or 7.28 x 10^{25} n/m^2, E > 50keV, 4.7dpa)
			12, Fig 11, Page 2435	Graph shows the fractional reduction in thermal conductivity as a function of neutron fluence for 222 (2.44 x 10^{25} n/m^2, E > 50 keV, 1.6 dpa or 7.28 x 10^{25} n/m^2, E > 50keV, 4.7dpa)
Volume Change			10, Fig 6, Page 987	Graph shows the radiation induced volume changes in 222 (2.44 x 10^{25} n/m^2, E > 50 keV, 1.6 dpa or 7.28 x 10^{25} n/m^2, E > 50keV, 4.7dpa)
Volume Change			11, Fig 5, Page 1273	Graph shows the radiation induced volume changes in 222 (2.44 x 10^{25} n/m^2, E > 50 keV, 1.6 dpa or 7.28 x 10^{25} n/m^2, E > 50keV, 4.7dpa)

A3 223

Mechanical Property	Value	Units	Reference	Notes
Diameter Change			10, Fig 5, Page 987	Graph shows the radiation induced diameter changes in 223 (2.44 x 10^{25} n/m^2, E > 50 keV, 1.6 dpa or 7.28 x 10^{25} n/m^2, E > 50keV, 4.7dpa)
Diameter Change			11, Fig 7, Page 1274	Graph shows the radiation induced diameter changes in 223 (2.44 x 10^{25} n/m^2, E > 50 keV, 1.6 dpa or 7.28 x 10^{25} n/m^2, E > 50keV, 4.7dpa)
Dimensional Changes			12, Fig 8 (a) & (b), Page 2434	Graphs show the irradiation dimensional change 223
Fractional Change in Strength	1.00		11, Table 2, Page 1276	Unirradiated at 2650°C
	1.77		11, Table 2, Page 1276	Irradiated at 2650°C and a fluence of 0.74 DPA - E > 50keV

Mechanical Property	Value	Units	Reference	Notes
	1.04		11, Table 2, Page 1276	Irradiated at 2650°C and a fluence of 2.20 DPA - E > 50keV
	1.00		11, Table 2, Page 1276	Unirradiated at 3100°C
	1.46		11, Table 2, Page 1276	Irradiated at 3100°C and a fluence of 0.81 DPA - E > 50keV
	1.25		11, Table 2, Page 1276	Irradiated at 3100°C and a fluence of 2.39 DPA - E > 50keV
Fracture Strength	90.9 ± 15.8	MPa	11, Table 2, Page 1276	Unirradiated at 2650°C
	160.9	MPa	11, Table 2, Page 1276	Irradiated at 2650°C and a fluence of 0.74 DPA - E > 50keV
	94.7	MPa	11, Table 2, Page 1276	Irradiated at 2650°C and a fluence of 2.20 DPA - E > 50keV
	89.6 ± 9.6	MPa	11, Table 2, Page 1276	Unirradiated at 3100°C
	131.1	MPa	11, Table 2, Page 1276	Irradiated at 3100°C and a fluence of 0.81 DPA - E > 50keV
	111.8	MPa	11, Table 2, Page 1276	Irradiated at 3100°C and a fluence of 2.39 DPA - E > 50keV
Length Change			10, Fig 4, Page 987	Graph shows the radiation induced length changes in 223 (2.44 x 10^{25} n/m^2, E > 50 keV, 1.6 dpa or 7.28 x 10^{25} n/m^2, E > 50keV, 4.7dpa)
Length Change			11, Fig 6, Page 1274	Graph shows the radiation induced length changes in 223 (2.44 x 10^{25} n/m^2, E > 50 keV, 1.6 dpa or 7.28 x 10^{25} n/m^2, E > 50keV, 4.7dpa)
Strength			11, Fig 9, Page 1277	Graph shows the effect of neutron irradiation on the strength of 223 - E > 50keV
Thermal Conductivity			11, Fig 10, Page 1279	Graph shows the effect of temperature in the themal conductivity of irradiated and unirradiated 223
			11, Fig 13, Page 1280	Graph shows the effect of post irradiation annealing on the thermal conductivity of 223 - E > 50keV
Thermal Conductivity			12, Fig 9, Page 2434	Graph shows the temperature dependence of thermal conductivity for 223
Volume Change			10, Fig 6, Page 987	Graph shows the radiation induced volume changes in 223 (2.44 x 10^{25} n/m^2, E > 50 keV, 1.6 dpa or 7.28 x 10^{25} n/m^2, E > 50keV, 4.7dpa)
Volume Change			11, Fig 5, Page 1273	Graph shows the radiation induced volume changes in 223 (2.44 x 10^{25} n/m^2, E > 50 keV, 1.6 dpa or 7.28 x 10^{25} n/m^2, E > 50keV, 4.7dpa)

A4 2D-C/C

Mechanical Property	Value	Units	Reference	Notes
Bending Strength	117	MPa	8, Table 1 (b), Page 1127	II unirradiated - makers data
	117	MPa	8, Table 3 (b), Page 1129	II unirradiated experimental results - mean values
	116	MPa	8, Table 3 (b), Page 1129	⊥ unirradiated experimental results - mean values
	117	MPa	8, Table 4 (b), Page 1131	II unirradiated experimental results - mean values
	145	MPa	8, Table 4 (b), Page 1131	II irradiated in JMTR up to 1.9 x 10^{21} n/cm^2 at 650 ~ 1000°C - mean values E > 29 fJ
	116	MPa	8, Table 4 (b), Page 1131	⊥ unirradiated experimental results - mean values
	143	MPa	8, Table 4 (b), Page 1131	⊥ irradiated in JMTR up to 1.9 x 10^{21} n/cm^2 at 650 ~ 1000°C - mean values E > 29 fJ
Bulk Density	1.74	g/cm^3	8, Table 1 (b), Page 1127	unirradiated - makers data
	1.74	g/cm^3	8, Table 3 (b), Page 1129	unirradiated experimental results - mean values
	1.74	g/cm^3	8, Table 4, Page 1131	unirradiated experimental results - mean values
	1.82	g/cm^3	8, Table 4, Page 1131	irradiated in JMTR up to 1.9 x 10^{21} n/cm^2 at 650 ~ 1000°C - mean values E > 29 fJ
Compressive Strength	44.1	MPa	8, Table 1 (b), Page 1127	II unirradiated - makers data
Dimensional Change	-1.54	%	8, Table 4, Page 1131	irradiated in JMTR up to 1.9 x 1021 n/cm2 at 650 ~ 1000°C - mean values E > 29 fJ
Electric Resistivity	1217	μΩcm	8, Table 4, Page 1131	unirradiated experimental results - mean values
	2323	μΩcm	8, Table 4, Page 1131	irradiated in JMTR up to 1.9 x 1021 n/cm2 at 650 ~ 1000°C - mean values E > 29 fJ
Fracture Toughness	5.26	MPa $m^{1/2}$	8, Table 3 (b), Page 1129	Mode 1 II unirradiated experimental results - mean values
	5.26	MPa $m^{1/2}$	8, Table 4 (b), Page 1131	Mode 1 II unirradiated experimental results - mean value
	5.77	MPa $m^{1/2}$	8, Table 4 (b), Page 1131	Mode 1 II irradiated in JMTR up to 1.9 x 1021 n/cm2 at 650 ~ 1000°C - mean values E > 29 fJ
Impact Absorbed Energy	1.54	J/cm^3	8, Table 4, Page 1131	II unirradiated experimental results - mean values
	1.66	J/cm^3	8, Table 4, Page 1131	II irradiated in JMTR up to 1.9 x 1021 n/cm2 at 650 ~ 1000°C - mean values E > 29 fJ
	1.54	J/cm^3	8, Table 4, Page 1131	⊥ unirradiated experimental results - mean values
	1.67	J/cm^3	8, Table 4, Page 1131	⊥ irradiated in JMTR up to 1.9 x 1021 n/cm2 at 650 ~ 1000°C - mean values E > 29 fJ
Rockwell Hardness	74.8		8, Table 3 (b), Page 1129	II unirradiated experimental results - mean values
	74.8		8, Table 4, Page 1131	unirradiated expermental results - mean values

Mechanical Property	Value	Units	Reference	Notes
	80.6		8, Table 4, Page 1131	irradiated in JMTR up to 1.9 x 1021 n/cm2 at 650 ~ 1000°C - mean values E > 29 fJ
Specific Heat	0.71	J/gK	8, Table 1 (b), Page 1127	II unirradiated - makers data
Tensile Strength	90.1	MPa	8, Table 4, Page 1131	unirradiated experimental results - mean values
	114	MPa	8, Table 4, Page 1131	irradiated in JMTR up to 1.9 x 1021 n/cm2 at 650 ~ 1000°C - mean values E > 29 fJ
Thermal Conductivity	419	W/mK	8, Table 1 (b), Page 1127	II unirradiated - makers data
Thermal Diffusivity	47.9	mm^2/s	8, Table 4 (b), Page 1131	unirradiated experimental results - mean values
	25.2	mm^2/s	8, Table 4 (b), Page 1131	irradiated in JMTR up to 1.9 x 1021 n/cm2 at 650 ~ 1000°C - mean values E > 29 fJ
Thermal Expansivity	0.72	$10^{-6}/K$	8, Table 1 (b), Page 1127	⊥ unirradiated - makers data
Thermal Shock Fracture Toughness	>856	$W/mm^{1/2}$	8, Table 3 (b), Page 1129	II unirradiated experimental results - mean values
	>856	$W/mm^{1/2}$	8, Table 4, Page 1131	unirradiated experimental results - mean values
	221	$W/mm^{1/2}$	8, Table 4, Page 1131	irradiated in JMTR up to 1.9 x 1021 n/cm2 at 650 ~ 1000°C - mean values E > 29 fJ
			8, Fig 4 (a), Page 1128	Graph shows the thermal shock fracture toughnesses of tested materials
			8, Fig 5 (a), Page 1132	Graph shows the thermal shock fracture toughnesses of tested materials before and after irradiation E > 29 fJ
Thermal Shock Resistance	>68.3	W/mm	8, Table 3 (b), Page 1129	II unirradiated experimental results - mean values
	>68.3	W/mm	8, Table 4, Page 1131	unirradiated experimental results - mean values
	75.5	W/mm	8, Table 4, Page 1131	irradiated in JMTR up to 1.9 x 1021 n/cm2 at 650 ~ 1000°C - mean values E > 29 fJ
			8, Fig 4 (a), Page 1128	Graph shows the thermal shock resistances of tested materials
			8, Fig 5 (a), Page 1132	Graph shows the thermal shock resistances of tested materials before and after irradiation E > 29 fJ
Total Porosity	14.2	%	8, Table 4, Page 1131	unirradiated experimental results - mean values
	10.2	%	8, Table 4, Page 1131	irradiated in JMTR up to 1.9 x 1021 n/cm2 at 650 ~ 1000°C - mean values E > 29 fJ
Young's Modulus	23.8	GPa	8, Table 1 (b), Page 1127	II unirradiated - makers data
	23.7	GPa	8, Table 3 (b), Page 1129	II unirradiated experimental results - mean values
	23.8	GPa	8, Table 4, Page 1131	unirradiated experimental results - mean values
	31.6	GPa	8, Table 4, Page 1131	irradiated in JMTR up to 1.9 x 1021 n/cm2 at 650 ~ 1000°C - mean values E > 29 fJ

A5 AC 250

Mechanical Property	Value	Units	Reference	Notes
Bending Strength (3 point)	85.2	MPa	14, Table A2, Page 32	Tests on 20 samples of AC250 UD at room temperature - mean value
	171.3	MPa	14, Table A2, Page 32	Tests on 20 samples of AC250 2D at room temperature - mean value
Compressive Strength	63.2	MPa	14, Table A2, Page 32	Tests on 20 samples of AC250 UD at room temperature - mean value
	194.8	MPa	14, Table A2, Page 32	Tests on 20 samples of AC250 2D at room temperature - mean value
Density	1.7	g/cm^3	14, Table A3, Page 33	Catalogue value for AC250 UD at room temperature
Electrical Resistivity	17	μΩm	14, Table A3, Page 33	Catalogue value for AC250 UD at room temperature
Shear Strength	36.6	MPa	14, Table A2, Page 32	Tests on 20 samples of AC250 UD at room temperature - mean value
	17.6	MPa	14, Table A2, Page 32	Tests on 20 samples of AC250 2D at room temperature - mean value
Specific Heat	0.75	J/gK	14, Table A3, Page 33	Catalogue values for AC250 UD at room temperature
	1.88	J/gK	14, Table A3, Page 33	Catalogue values for AC250 UD at 1200°C
Tensile Strength	103.5	MPa	14, Table A2, Page 32	Tests on 20 samples of AC250 UD at room temperature - mean value
	131.9	MPa	14, Table A2, Page 32	Tests on 20 samples of AC250 2D at room temperature - mean value
Thermal Conductivity	68.6	W/mK	14, Table A3, Page 33	Catalogue values for AC250 UD parallel
	10.5	W/mK	14, Table A3, Page 33	Catalogue values for AC250 UD transverse
Thermal Expansion Coefficient	0.6	$10^{-6}/K$	14, Table A3, Page 33	Catalogue values for AC250 UD parallel
	8.2	$10^{-6}/K$	14, Table A3, Page 33	Catalogue values for AC250 UD transverse
Young's Modulus	103.5	GPa	14, Table A2, Page 32	Tests on 20 samples of AC250 UD at room temperature (Tensile)
	85.2	GPa	14, Table A2, Page 32	Tests on 20 samples of AC250 UD at room temperature (Bending)

A6 A05

Mechanical Property	Value	Units	Reference	Notes
Density	1.87	g/cm^3	4, Table 1 Page 1168	unirradiated
Diameter Change			10, Fig 2, Page 987	Graph shows the radiation induced diameter changes in A05 - irradiated in HFIR 1 or 2 (2.44 x 10^{25} n/m^2, E > 50 keV, 1.6 dpa or 7.28 x 10^{25} n/m^2, E > 50keV, 4.7dpa)
Diameter Change			11, Fig 2, Page 1270	Graph shows the radiation induced diameter changes in A05 - irradiated in HFIR 1 or 2 (2.44 x 10^{25} n/m^2, E > 50 keV, 1.6 dpa or 7.28 x 10^{25} n/m^2, E > 50keV, 4.7dpa)

Mechanical Property	Value	Units	Reference	Notes
Length Change			10, Fig 1, Page 987	Graph shows the radiation induced length changes in A05 - irradiated in HFIR 1 or 2 (2.44 x 10^{25} n/m^2, E > 50 keV, 1.6 dpa or 7.28 x 10^{25} n/m^2, E > 50keV, 4.7dpa)
Length Change			11, Fig 1, Page 1270	Graph shows the radiation induced length changes in A05 - irradiated in HFIR 1 or 2 (2.44 x 10^{25} n/m^2, E > 50 keV, 1.6 dpa or 7.28 x 10^{25} n/m^2, E > 50keV, 4.7dpa)
Volume Change			10, Fig 3, Page 987	Graph shows the radiation induced volume changes in A05 - irradiated in HFIR 1 or 2 (2.44 x 10^{25} n/m^2, E > 50 keV, 1.6 dpa or 7.28 x 10^{25} n/m^2, E > 50keV, 4.7dpa)
Volume Change			11, Fig 4, Page 1273	Graph shows the radiation induced volume changes in A05 - irradiated in HFIR 1 or 2 (2.44 x 10^{25} n/m^2, E > 50 keV, 1.6 dpa or 7.28 x 10^{25} n/m^2, E > 50keV, 4.7dpa)
Thermal Conductivity	149	W/mK	6, Table 1 Page 1168	unirradiated, T = 400°C
	117	W/mK	6, Table 1 Page 1168	unirradiated, T = 600°C
	87.3	W/m°C	6, Table 5, Page 1172	T = 100°C / Sample 20G, GRIPS irradiated, T = 400°C/0.1dpa E > 0.1 MeV
	89.4	W/m°C	6, Table 5, Page 1172	T = 200°C / Sample 20G, GRIPS irradiated, T = 400°C/0.1dpa E > 0.1 MeV
	86.2	W/m°C	6, Table 5, Page 1172	T = 300°C / Sample 20G, GRIPS irradiated, T = 400°C/0.1dpa E > 0.1 MeV
	80.6	W/m°C	6, Table 5, Page 1172	T = 400°C / Sample 20G, GRIPS irradiated, T = 400°C/0.1dpa E > 0.1 MeV
	103.7	W/m°C	6, Table 5, Page 1172	T = 100°C / Sample 5G, GRIPS irradiated, T = 600°C/0.1dpa E > 0.1 MeV
	103.3	W/m°C	6, Table 5, Page 1172	T = 200°C / Sample 5G, GRIPS irradiated, T = 600°C/0.1dpa E > 0.1 MeV
	98.2	W/m°C	6, Table 5, Page 1172	T = 300°C / Sample 5G, GRIPS irradiated, T = 600°C/0.1dpa E > 0.1 MeV
	91.1	W/m°C	6, Table 5, Page 1172	T = 400°C / Sample 5G, GRIPS irradiated, T = 600°C/0.1dpa E > 0.1 MeV
	83.8	W/m°C	6, Table 5, Page 1172	T = 500°C / Sample 5G, GRIPS irradiated, T = 600°C/0.1dpa E > 0.1 MeV
	77	W/m°C	6, Table 5, Page 1172	T = 600°C / Sample 5G, GRIPS irradiated, T = 600°C/0.1dpa E > 0.1 MeV
			6, Fig 2, Page 1173	Graphs show the normalised thermal conductivity of various carbon-carbon composites as a function of neutron dose at irradiation temperatures 400° and 600°C E > 0.1 MeV
Thermal Diffusivity			4, Fig 2, Page 301	Graph shows the irradiation induced changes in thermal diffusivity of A05 E > 29 fJ
			4, Fig 4, Page 302	Graph shows changes in the temperature dependence of the normalised thermal diffusivity of the material at four measurement temperatures as a function neutron fluence E > 29 fJ
			4, Fig 6, Page 302	Graph shows the changes in normalised thermal diffusivity of the material at four measurement temperatures as a function of neutron fluence E > 29 fJ
	53.4	mm^2/s	6, Table 5, Page 1172	T = 100°C / Sample 20G, GRIPS irradiated, T = 400°C/0.1dpa E > 0.1 MeV

Mechanical Property	Value	Units	Reference	Notes
	42.9	mm^2/s	6, Table 5, Page 1172	T = 200°C / Sample 20G, GRIPS irradiated, T = 400°C/0.1dpa E > 0.1 MeV
	35.8	mm^2/s	6, Table 5, Page 1172	T = 300°C / Sample 20G, GRIPS irradiated, T = 400°C/0.1dpa E > 0.1 MeV
	30.5	mm^2/s	6, Table 5, Page 1172	T = 400°C / Sample 20G, GRIPS irradiated, T = 400°C/0.1dpa E > 0.1 MeV
	63.9	mm^2/s	6, Table 5, Page 1172	T = 100°C / Sample 5G, GRIPS irradiated, T = 600°C/0.1dpa E > 0.1 MeV
	50.0	mm^2/s	6, Table 5, Page 1172	T = 200°C / Sample 5G, GRIPS irradiated, T = 600°C/0.1dpa E > 0.1 MeV
	41.0	mm^2/s	6, Table 5, Page 1172	T = 300°C / Sample 5G, GRIPS irradiated, T = 600°C/0.1dpa E > 0.1 MeV
	34.8	mm^2/s	6, Table 5, Page 1172	T = 400°C / Sample 5G, GRIPS irradiated, T = 600°C/0.1dpa E > 0.1 MeV
	30.2	mm^2/s	6, Table 5, Page 1172	T = 500°C / Sample 5G, GRIPS irradiated, T = 600°C/0.1dpa E > 0.1 MeV
	26.6	mm^2/s	6, Table 5, Page 1172	T = 600°C / Sample 5G, GRIPS irradiated, T = 600°C/0.1dpa E > 0.1 MeV

A7 C/C-A

Mechanical Property	Value	Units	Reference	Notes
Ash Content	<20	ppm	8, Table 1 (b), Page 1127	unirradiated physical properties - makers data
Bending Strength	65.7	MPa	8, Table 1 (b), Page 1127	II unirradiated physical properties - makers data
	65.7	MPa	8, Table 3 (b), Page 1129	II unirradiated experimental results
	57.4	MPa	8, Table 3 (b), Page 1129	⊥ unirradiated experimental results
	65.7	MPa	8, Table 4, Page 1131	II unirradiated experimental results - mean values
	81.5	MPa	8, Table 4, Page 1131	II irradiated in JMTR up to 1.9 x 10^{21} n/cm^2 at 650 ~ 1000°C - mean values E > 29 fJ
	57.4	MPa	8, Table 4, Page 1131	⊥ unirradiated experimental results - mean values
	79.8	MPa	8, Table 4, Page 1131	⊥ irradiated in JMTR up to 1.9 x 10^{21} n/cm^2 at 650 ~ 1000°C - mean values E > 29 fJ
Bulk Density	1.58	g/cm^3	8, Table 1 (b), Page 1127	unirradiated physical properties - makers data
	1.58	g/cm^3	8, Table 3 (b), Page 1129	unirradiated experimental results
	2.58	g/cm^3	8, Table 4 (b), Page 1129	unirradiated experimental results
	1.60	g/cm^3	8, Table 4, Page 1131	irradiated in JMTR up to 1.9 x 10^{21} n/cm^2 at 650 ~ 1000°C - mean values E > 29 fJ
Compressive Strength	44.9	MPa	8, Table 4, Page 1131	unirradiated experimental results - mean values
	58.4	MPa	8, Table 4, Page 1131	irradiated in JMTR up to 1.9 x 1021 n/cm2 at 650 ~ 1000°C - mean values E > 29 fJ
Dimensional Change	-0.37	%	8, Table 4, Page 1131	irradiated in JMTR up to 1.9 x 1021 n/cm2 at 650 ~ 1000°C - mean values E > 29 fJ

Mechanical Property	Value	Units	Reference	Notes
Fracture Toughness	2.96	MPa $m^{1/2}$	8, Table 3 (b), Page 1129	Mode 1 II unirradiated experimental results
	2.14	MPa $m^{1/2}$	8, Table 3 (b), Page 1129	Mode 1 ⊥ unirradiated experimental results
	3.79	MPa $m^{1/2}$	8, Table 3 (b), Page 1129	Mode 2 II unirradiated experimental results
	2.96	MPa $m^{1/2}$	8, Table 4, Page 1131	Mode 1 II unirradiated experimental results - mean value
	3.65	MPa $m^{1/2}$	8, Table 4, Page 1131	Mode 1 II irradiated in JMTR up to 1.9 x 1021 n/cm2 at 650 ~ 1000°C - mean values E > 29 fJ
	2.14	MPa $m^{1/2}$	8, Table 4, Page 1131	Mode 1 ⊥ unirradiated experimental results - mean value
	2.65	MPa $m^{1/2}$	8, Table 4, Page 1131	Mode 1 ⊥ II irradiated in JMTR up to 1.9 x 1021 n/cm2 at 650 ~ 1000°C - mean values E > 29 fJ
	3.79	MPa $m^{1/2}$	8, Table 4, Page 1131	Mode 2 unirradiated experimental results - mean values
	4.85	MPa $m^{1/2}$	8, Table 4, Page 1131	Mode 2 irradiated in JMTR up to 1.9 x 1021 n/cm2 at 650 ~ 1000°C - mean values E > 29 fJ
Impact Absorbed Energy	1.23	J/cm^2	8, Table 4, Page 1131	II unirradiated experimental results - mean values
	1.28	J/cm^2	8, Table 4, Page 1131	II irradiated in JMTR up to 1.9 x 1021 n/cm2 at 650 ~ 1000°C - mean values E > 29 fJ
	1.22	J/cm^2	8, Table 4, Page 1131	⊥ unirradiated experimental results - mean values
	1.28	J/cm^2	8, Table 4, Page 1131	⊥ ιρραδιατεδ ιν ϑMTP υπ το 1.9 ξ 1021 ν/χμ2 ατ 650 ~ 1000°X – μεαν ϖαλυεσ E > 29 φϑ
Rockwell Hardness	42.0		8, Table 3 (b), Page 1129	II unirradiated experimental results
	42		8, Table 4, Page 1131	unirradiated experimental results - mean values
	50		8, Table 4, Page 1131	irradiated in JMTR up to 1.9 x 1021 n/cm2 at 650 ~ 1000°C - mean values E > 29 fJ
Tensile Strength	35.7	MPa	8, Table 4, Page 1131	unirradiated experimental results - mean values
Thermal Diffusivity	62.4	mm^2/s	8, Table 4, Page 1131	unirradiated experimental results - mean values
	48.5	mm^2/s	8, Table 4, Page 1131	irradiated in JMTR up to 1.9 x 1021 n/cm2 at 650 ~ 1000°C - mean values E > 29 fJ
Thermal Shock Fracture Toughness	739	W/$mm^{1/2}$	8, Table 3 (b), Page 1129	II unirradiated experimental results
	739	W/$mm^{1/2}$	8, Table 4, Page 1131	unirradiated experimental results - mean values
	>356	W/$mm^{1/2}$	8, Table 4, Page 1131	irradiated in JMTR up to 1.9 x 1021 n/cm2 at 650 ~ 1000°C - mean values E > 29 fJ
			8, Fig 4 (b), Page 1128	Graph shows the thermal shock fracture toughnesses of tested materials E > 29 fJ
			8, Fig 5 (b), Page 1132	Graph shows the thermal shock fracture toughnesses of tested materials before and after irradiation E > 29 fJ

Mechanical Property	Value	Units	Reference	Notes
Thermal Shock Resistance	>194	W/mm	8, Table 3 (b), Page 1129	II unirradiated experimental results
	>194	W/mm	8, Table 4, Page 1131	unirradiated experimental results - mean values
	>97	W/mm	8, Table 4, Page 1131	irradiated in JMTR up to 1.9 x 1021 n/cm2 at 650 ~ 1000°C - mean values E > 29 fJ
			8, Fig 4 (b), Page 1128	Graph shows the thermal shock resistances of tested materials before and after irradiation
			8, Fig 5 (a), Page 1132	Graph shows the thermal shock resistances of tested materials before and after irradiation E > 29 fJ
Total Porosity	30.1	%	8, Table 4, Page 1131	unirradiated experimental results - mean values
	29.2	%	8, Table 4, Page 1131	irradiated in JMTR up to 1.9 x 1021 n/cm2 at 650 ~ 1000°C - mean values E > 29 fJ
Young's Modulus	13.5	GPa	8, Table 1 (b), Page 1127	II unirradiated physical properties - makers data
	13.5	GPa	8, Table 3 (b), Page 1129	II unirradiated experimental results
	13.5	GPa	8, Table 4, Page 1131	unirradiated experimental results - mean values
	19.2	GPa	8, Table 4, Page 1131	irradiated in JMTR up to 1.9 x 1021 n/cm2 at 650 ~ 1000°C - mean values E > 29 fJ

A8 C/C –B

Mechanical Property	Value	Units	Reference	Notes
Ash Content	<20	ppm	8, Table 1 (b), Page 1127	unirradiated - makers data
Bending Strength	90.0	MPa	8, Table 1 (b), Page 1127	II unirradiated - makers data
	96.9	MPa	8, Table 3 (b), Page 1129	II unirradiated experimental results - mean values
	94.5	MPa	8, Table 3 (b), Page 1129	⊥ unirradiated experimental results - mean values
	96.9	MPa	8, Table 4 (b), Page 1131	II unirradiated experimental results - mean values
	119.2	MPa	8, Table 4 (b), Page 1131	II irradiated in JMTR up to 1.9 x 1021 n/cm2 at 650 ~ 1000°C - mean values E > 29 fJ
	94.5	MPa	8, Table 4 (b), Page 1131	⊥ unirradiated experimental results - mean values
	110.0	MPa	8, Table 4 (b), Page 1131	^ irradiated in JMTR up to 1.9 x 1021 n/cm2 at 650 ~ 1000°C - mean values E > 29 fJ
Bulk Density	1.75	g/cm^3	8, Table 1 (b), Page 1127	unirradiated - makers data
	1.77	g/cm^3	8, Table 3 (b), Page 1129	unirradiated experimental results - mean values
	1.77	g/cm^3	8, Table 4 (b), Page 1131	unirradiated experimental results - mean values

Mechanical Property	Value	Units	Reference	Notes
	1.80	g/cm^3	8, Table 4 (b), Page 1131	irradiated in JMTR up to 1.9 x 1021 n/cm2 at 650 ~ 1000°C - mean values E > 29 fJ
Compressive Strength	80	MPa	8, Table 1 (b), Page 1127	II unirradiated - makers data
	66.3	MPa	8, Table 4 (b), Page 1131	unirradiated experimental results - mean values
	81.2	MPa	8, Table 4 (b), Page 1131	irradiated in JMTR up to 1.9 x 1021 n/cm2 at 650 ~ 1000°C - mean values E > 29 fJ
Dimensional Change	-0.64	%	8, Table 4 (b), Page 1131	irradiated in JMTR up to 1.9 x 1021 n/cm2 at 650 ~ 1000°C - mean values E > 29 fJ
Electric Resistivity	400	μΩcm	8, Table 1 (b), Page 1127	II unirradiated - makers data
	700	μΩcm	8, Table 1 (b), Page 1127	⊥ unirradiated - makers data
	400	μΩcm	8, Table 4 (b), Page 1131	unirradiated experimental results - mean values
	580	μΩcm	8, Table 4 (b), Page 1131	irradiated in JMTR up to 1.9 x 1021 n/cm2 at 650 ~ 1000°C - mean values E > 29 fJ
Fracture Toughness	3.44	MPa $m^{1/2}$	8, Table 3 (b), Page 1129	Mode 1 II unirradiated experimental results - mean values
	3.03	MPa $m^{1/2}$	8, Table 3 (b), Page 1129	Mode 1 ⊥ unirradiated experimental results - mean values
	4.39	MPa $m^{1/2}$	8, Table 3 (b), Page 1129	Mode 2 II unirradiated experimental results - mean values
	3.44	MPa $m^{1/2}$	8, Table 4 (b), Page 1131	Mode 1 II unirradiated experimental results - mean value
	4.14	MPa $m^{1/2}$	8, Table 4 (b), Page 1131	Mode 1 II irradiated in JMTR up to 1.9 x 1021 n/cm2 at 650 ~ 1000°C - mean values E > 29 fJ
	3.03	MPa $m^{1/2}$	8, Table 4 (b), Page 1131	Mode 1 ⊥ unirradiated experimental results - mean value
	3.94	MPa $m^{1/2}$	8, Table 4 (b), Page 1131	Mode 1 ^ II irradiated in JMTR up to 1.9 x 1021 n/cm2 at 650 ~ 1000°C - mean values E > 29 fJ
	4.39	MPa $m^{1/2}$	8, Table 4 (b), Page 1131	Mode 2 unirradiated experimental results - mean values
	5.56	MPa $m^{1/2}$	8, Table 4 (b), Page 1131	Mode 2 irradiated in JMTR up to 1.9 x 1021 n/cm2 at 650 ~ 1000°C - mean values E > 29 fJ
Impact Absorbed Energy	1.16	J/cm^2	8, Table 4 (b), Page 1131	II unirradiated experimental results - mean values
	1.18	J/cm^2	8, Table 4 (b), Page 1131	II irradiated in JMTR up to 1.9 x 1021 n/cm2 at 650 ~ 1000°C - mean values E > 29 fJ
	1.13	J/cm^2	8, Table 4 (b), Page 1131	⊥ unirradiated experimental results - mean values
	1.16	J/cm^2	8, Table 4 (b), Page 1131	^ irradiated in JMTR up to 1.9 x 1021 n/cm2 at 650 ~ 1000°C - mean values E > 29 fJ

Mechanical Property	Value	Units	Reference	Notes
Rockwell Hardness	44.0		8, Table 3, (b), Page 1129	II unirradiated experimental results - mean values
	44		8, Table 4 (b), Page 1131	unirradiated experimental results - mean values
	58		8, Table 4 (b), Page 1131	irradiated in JMTR up to 1.9 x 1021 n/cm2 at 650 ~ 1000°C - mean values E > 29 fJ
Shore Hardness	30		8, Table 1 (b), Page 1127	II unirradiated - makers data
Specific Heat	0.70	J/gK	8, Table 1 (b), Page 1127	II unirradiated - makers data
Tensile Strength	55.4	MPa	8, Table 4 (b), Page 1131	unirradiated experimental results - mean values
Thermal Conductivity	150	W/mK	8, Table 1 (b), Page 1127	II unirradiated - makers data *adjusted from table
	100	W/mK	8, Table 1 (b), Page 1127	⊥ unirradiated - makers data *adjusted from table
Thermal Diffusivity	56.6	mm^2/s	8, Table 4 (b), Page 1131	unirradiated experimental results - mean values
	45.3	mm^2/s	8, Table 4 (b), Page 1131	irradiated in JMTR up to 1.9 x 1021 n/cm2 at 650 ~ 1000°C - mean values E > 29 fJ
Thermal Expansivity	1.0	$10^{-6}/K$	8, Table 1 (b), Page 1127	⊥ unirradiated - makers data
	8.0	$10^{-6}/K$	8, Table 1 (b), Page 1127	II unirradiated - makers data
Thermal Shock Fracture Toughness	196	$W/mm^{1/2}$	8, Table 3 (b), Page 1129	II unirradiated experimental results - mean values
	196	$W/mm^{1/2}$	8, Table 4 (b), Page 1131	unirradiated experimental results - mean values
	164	$W/mm^{1/2}$	8, Table 4 (b), Page 1131	irradiated in JMTR up to 1.9 x 1021 n/cm2 at 650 ~ 1000°C - mean values E > 29 fJ
			8, Fig 4 (b), Page 1128	Graph shows the thermal shock fracture toughnesses of tested materials
			8, Fig 5 (b), Page 1132	Graph shows the thermal shock fracture toughnesses of tested materials before and after irradiation
Thermal Shock Resistance	>194	W/mm	8, Table 3 (b), Page 1129	II unirradiated experimental results - mean values
	>194	W/mm	8, Table 4 (b), Page 1131	unirradiated experimental results - mean values
	>94	W/mm	8, Table 4 (b), Page 1131	irradiated in JMTR up to 1.9 x 1021 n/cm2 at 650 ~ 1000°C - mean values E > 29 fJ
			8, Fig 4 (a), Page 1128	Graph shows the thermal shock resistances of tested materials
			8, Fig 5 (a), Page 1132	Graph shows the thermal shock resistances of tested materials before and after irradiation
Total Porosity	21.7	%	8, Table 4 (b), Page 1131	unirradiated experimental results - mean values

Mechanical Property	Value	Units	Reference	Notes
	20.4	%	8, Table 4 (b), Page 1131	irradiated in JMTR up to 1.9 x 1021 n/cm2 at 650 ~ 1000°C - mean values E > 29 fJ
Young's Modulus	26.0	GPa	8, Table 1 (b), Page 1127	II unirradiated - makers data
	26.3	GPa	8, Table 3 (b), Page 1129	II unirradiated experimental results - mean values
	26.3	GPa	8, Table 4 (b), Page 1131	unirradiated experimental results - mean values
	34.2	GPa	8, Table 4 (b), Page 1131	irradiated in JMTR up to 1.9 x 1021 n/cm2 at 650 ~ 1000°C - mean values E > 29 fJ

A9 CC 2001 G

Mechanical Property	Value	Units	Reference	Notes
Bending Strength	280 - 350	MPa	13, Fig 2, Page 60	Technical Data
Density	1.3 - 1.5	g/cm^3	13, Fig 2, Page 60	Technical Data
Stress/Strain			13, Fig 5, Page 61	Stress/Strain diagram
			13, Fig 7, Page 62	Axial Stress
			13, Fig 8, Page 63	Axial Stress
Tensile Strength	380 - 470	MPa	13, Fig 2, Page 60	Technical Data
Youngs Modulus	110 - 130	GPa	13, Fig 2, Page 60	Technical Data

A10 CX 270

Mechanical Property	Value	Units	Reference	Notes
Bending Strength (3 point)	169.0	MPa	14, Table A2, Page 32	Tests on 50 samples at room temperature - mean values
Compressive Strength	88.0	MPa	14, Table A2, Page 32	Tests on 50 samples at room temperature - mean values (parallel)
	226	MPa	14, Table A2, Page 32	Tests on 50 samples at room temperature - mean values (transverse)
Density	1.592 ± 0.024	g/cm^3	14, Table A3, Page 33	Tests on 50 samples at room temperature - mean values
Electrical Resistivity	17.1 ± 0.33	$\mu\Omega m$	14, Table A3, Page 34	Tests on 50 samples at room temperature - mean values
Tensile Strength	227	MPa	14, Table A2, Page 32	Catalogue value
Thermal Conductivity	35	W/mK	14, Table A3, Page 33	Catalogue values for CX 270 parallel
	5	W/mK	14, Table A3, Page 33	Catalogue values for CX 270 transverse
Thermal Expansion Coefficient	<1	$10^{-6}/K$	14, Table A3, Page 33	Catalogue value
	8	$10^{-6}/K$	14, Table A3, Page 33	Catalogue value
Young's Modulus	102	GPa	14, Table A2,	Catalogue value

Mechanical Property	Value	Units	Reference	Notes
			Page 32	

A11 CX-2002U

Mechanical Property	Value	Units	Reference	Notes
Ash Content	<10	ppm	8, Table 1(b), Page 1127	unirradiated (makers data)
Bending Fracture Strain	0.440 ± 0.085	%	7, Table 3, Page 1225	unirradiated
	46.7 ± 0.08	%	7, Table 3, Page 1225	irradiated in the JMTR at ~ 1000°C & up to 2 x 10^{25} n/m^2 E > 29 fJ
Bending Fracture Strain	0.44 (X)	%	9, Table 1, Page 11	unirradiated
Bending Strength	44	MPa	3, Table 1, Page 45	unirradiated
Bending Strength	44	MPa	7, Table 1, Page 1224	II typical properties
	36.3 ± 3.9	MPa	7, Table 3, Page 1225	unirradiated
	46.7 ± 2.6	MPa	7, Table 3, Page 1225	irradiated in the JMTR at ~ 1000°C & up to 2 x 10^{25} n/m^2 E > 29 fJ
			7, Fig 4, Page 1226	Graph shows the stress-strain curves obtained during the bending test of CX-2002U before and after irradiation
Bending Strength	54.9	MPa	8, Table 1(b), Page 1127	II to moulding direction, unirradiated (makers data)
	49	MPa	8, Table 1(b), Page 1127	⊥ to moulding direction, unirradiated (makers data)
Bending Strength	36.3 (X)	MPa	9, Table 1, Page 11	unirradiated
			9, Fig 10, Page 15	Graph shows the bending stress- strain curves of carbon materials before and after irradiation at 1.3 x 10^{25} n/m^2 E > 0.18MeV
Bulk Density	1.72	g/cm^3	8, Table 1(b), Page 1127	unirradiated (makers data)
Compressive Fracture Strain	1.94 ± 0.82	%	7, Table 3, Page 1225	unirradiated
	1.82 ± 1.24	%	7, Table 3, Page 1225	irradiated in the JMTR at ~ 1000°C & up to 2 x 10^{25} n/m^2 E > 29 fJ
Compressive Fracture Strain	1.94 (X)	%	9, Table 1, Page 11	unirradiated
Compressive Strength	50 33.3 ± 8.7	MPa MPa	7, Table 1, Page 1224 7, Table 3, Page 1225	II typical properties unirradiated
	41.2 ± 9.2	MPa	7, Table 3, Page 1225	irradiated in the JMTR at ~ 1000°C & up to 2 x 10^{25} n/m^2 E > 29 fJ
			7, Fig 5, Page 1226	Graph shows the compressive stress-strain curves for CX-2002U before and after irradiation

Mechanical Property	Value	Units	Reference	Notes
Compressive Strength	61.7	MPa	8, Table 1(b), Page 1127	II to moulding direction, unirradiated (makers data)
	52.9	MPa	8, Table 1(b), Page 1127	⊥ to moulding direction, unirradiated (makers data)
Compressive Strength	33.3 (X)	MPa	9, Table 1, Page 11	unirradiated
Constant Of Thermal Expansion	2.6	(10^{-6}/K) T = 350 - 450°C	3, Table 1, Page 45	unirradiated
CTE	2.0	(10^{-6}/K)	7, Table 1, Page 1224	II typical properties
	5.7	(10^{-6}/K)	7, Table 1, Page 1224	⊥ typical properties
Density	1.65	g/cm^3	3, Table 1, Page 45	unirradiated
Density	1.60	g/cm^3	9, Table 1, Page 11	unirradiated
Apparent Density	1.65	g/cm^3	7, Table 1, Page 1224	⊥ typical properties
Dimensional Changes	0.03	%	3, Table 4, Page 46	irradiated at 0.01 dpa, 20°C
	-0.02	%	3, Table 4, Page 46	irradiated at 0.13 dpa, 300°C
	-0.27	%	3, Table 4, Page 46	irradiated at 0.82 dpa, 4300°C
Length Changes	-0.195	l/l_o (%)	7, Table 2, Page 1224	irradiated in the JMTR at ~ 1000°C & up to 2 x 10^{25} n/m^2. The values are the means of 2 or 4 specimens
Volume Changes	-2.06	V/V_o (%)	7, Table 2, Page 1224	irradiated in the JMTR at ~ 1000°C & up to 2 x 10^{25} n/m^2. The values are the means of 2 or 4 specimens
Dimensional Changes			9, Fig 6, Page 13	Graph shows the dimensional changes of carbon-carbon materials after irradiation at 1.3 x 10^{25} n/m^2 E > 0.18MeV
Electric Resistivity	440	μΩcm	8, Table 1(b), Page 1127	II to moulding direction, unirradiated (makers data)
Electrical Resistivity	3.50	μΩcm	9, Table 1, Page 11	unirradiated
Fibre Content	10	%	9, Table 1, Page 11	unirradiated
Modulus of Elasticity	12	GPa	3, Table 1, Page 45	unirradiated
Shore Hardness	35		8, Table 1(b), Page 1127	II to moulding direction, unirradiated (makers data)
	30		8, Table 1(b), Page 1127	⊥ to moulding direction, unirradiated (makers data)
Specific Heat	0.76	J/gK	8, Table 1(b), Page 1127	II to moulding direction, unirradiated (makers data)
Tensile Strength	30	MPa	3, Table 1, Page 45	unirradiated
Tensile Strength	30	MPa	7, Table 1, Page 1224	II typical properties
Thermal Conductivity	280	W/(mK) at T = 20°C	3, Table 1, Page 45	unirradiated
	9.8	W/(mK)	3, Table 4, Page 46	irradiated at 0.01 dpa, 20°C
	24.7	W/(mK)	3, Table 4, Page 46	irradiated at 0.82 dpa, 4300°C

Mechanical Property	Value	Units	Reference	Notes
			3, Fig 3, Page 48	Graph shows the post irradiation annealing and the thermal conductivity of the neutron irradiated C/C composite CX 2002 U
Thermal Conductivity	267	W/mK	8, Table 1(b), Page 1127	II to moulding direction, unirradiated (makers data)
	128	W/mK	8, Table 1(b), Page 1127	⊥ to moulding direction, unirradiated (makers data)
Thermal Conductivity	398 (X)	W/mK	9, Table 1, Page 11	II unirradiated (RT)
	205 (Y)	W/mK	9, Table 1, Page 11	⊥ unirradiated (RT)
Thermal Conductivity	330	W/mK	7, Table 1, Page 1224	II typical properties (RT)
	3	W/mK	7, Table 1, Page 1224	⊥ typical properties (RT)
Thermal Expansivity	1.9 (X)	10^{-6}/K	8, Table 1(b), Page 1127	II to moulding direction, unirradiated (makers data)
	6.7 (Y)	10^{-6}/K	8, Table 1(b), Page 1127	⊥ to moulding direction, unirradiated (makers data)
Thermal Expensivity	1.9 (X)	10^{-6}/°C	9, Table 1, Page 11	unirradiated
	6.7 (Y)	10^{-6}/°C	9, Table 1, Page 11	unirradiated
Young's Modulus	10	GPa	7, Table 1, Page 1224	II typical properties
	14.9	GPa	7, Table 3, Page 1225	unirradiated
	18.5	GPa	7, Table 3, Page 1225	irradiated in the JMTR at ~ 1000°C & up to 2 x 10^{25} n/m^2 E > 29 fJ
Young's Modulus	11.3	GPa	8, Table 1(b), Page 1127	unirradiated (makers data)
Young's Modulus	14.9 (X)	GPa	9, Table 1, Page 11	unirradiated
			9, Fig 5, Page 13	Graph shows Young's modulus using an ultra sonic method and by stress-strain curves - following irradiation at 1.3 x 10^{25} n/m^2 E > 0.18MeV
			9, Fig 7, Page 14	Graph shows the changes in Young's modulus of carbon materials following neutron irradiation at 1.3 x 10^{25} n/m^2 E > 0.18MeV

A12 DMS 678

Mechanical Property	Value	Units	Reference	Notes
Thermal conductivity	130	W/mK	6, Table 1, Page 1168	unirradiated, T = 400°C
	103	W/mK	6, Table 1, Page 1168	unirradiated, T = 600°C

			6, Fig 2, Page 1173	Graphs show the normalised thermal conductivity of various carbon-carbon composites as a function of neutron dose at irradiation temperatures 400° and 600°C E > 0.1 MeV
Density	1.82	g/cm^3	6, Table 1, Page 1168	unirradiated

A13 FMI 4D

Mechanical Property	Value	Units	Reference	Notes
Thermal conductivity	65	W/mK	6, Table 1, Page 1168	unirradiated, T = 400°C
	55	W/mK	6, Table 1, Page 1168	unirradiated, T = 600°C
			6, Fig 2, Page 11	Graphs show the normalised thermal conductivity of various carbon-carbon composites as a function of neutron dose at irradiation temperatures 400° and 600°C E > 0.1 MeV
Density	1.79	g/cm^3	6, Table 1, Page 1168	unirradiated

A14 MCI

Mechanical Property	Value	Units	Reference	Notes
Bending Fracture Strain	0.32 (X)	%	9, Table 1, Page 11	Mechanical properties - unirradiated
			9, Fig 9, Page 15	Graph shows the changes in the bending fracture strain of graphite materials following irradiation (2 x 10^{25} n/m^2 and 1200°C E > 0.18 MeV)
Bending Strength	103.9 (X)	MPa	9, Table 1, Page 11	Mechanical properties - unirradiated
			9, Fig 8, Page 14	Graph shows the changes in the bending strength following irradiation (2 x 10^{25} n/m^2 and 1200°CE > 0.18 MeV)
Compressive Fracture Strain	0.17 (X) 3.90 (Y)	%	9, Table 1, Page 11	Mechanical properties - unirradiated
Compressive Strength	59.8 (X) 48.5 (X)	MPa	9, Table 1, Page 11	Mechanical properties - unirradiated
Density	1.92	g/cm^3	9, Table 1, Page 11	Mechanical properties - unirradiated
Dimensional Changes			9, Fig 6, Page 13	Graph shows the dimensional changes of the materials following irradiation (2 x 10^{25} n/m^2 and 1200°CE > 0.18 MeV)
Fibre Content	40~50	%	9, Table 1, Page 11	Mechanical properties - unirradiated
Thermal Conductivity	339 (X) 58 (Y)	W/mK	9, Table 1, Page 11	Mechanical properties - unirradiated
Thermal Expansivity	0.12 (X) 10.0 (Y)	10^{-6}/C	9, Table 1, Page 11	Mechanical properties - unirradiated
Young's Modulus	136.5 (X)	GPa	9, Table 1, Page 11	Mechanical properties - unirradiated

			9, Fig 5, Page 13	Graph shows Youngs modulus using an ultra sonic method and stress strain curves
			9, Fig 7, Page 14	Graphs show the change in Youngs modulus following irradiation (2 x 10^{25} n/m^2 and 1200°C E > 0.18 MeV)

A15 MFC-1

Mechanical Property	Value	Units	Reference	Notes
Bending Fracture Strain	0.322 ± 0.133 (X) 0.312 ± 0.58 (Y) 0.294 ± 0.141 (Z)	%	7, Table 3, Page 1225	unirradiated - measured
	0.2 ± 0.101 (X) 0.325 ± 0.7 (Z)	%	7, Table 3, Page 1225	2 x 10^{25} n/m^2 E > 29fJ irradiated - measured
Bending Strength	250	MPa	7, Table 1, Page 1224	II unirradiated - typical properties
	8	MPa	7, Table 1, Page 1224	⊥ unirradiated - typical properties
	103.9 ± 6.8 (X) 5.8 ± 2.5 (Y) 99.2 ± 17.6 (Z)	MPa	7, Table 3, Page 1225	unirradiated - measured
	98.4 ± 2.7 (X) 88.9 ± 8.2 (Z)	MPa	7, Table 3, Page 1225	2 x 10^{25} n/m^2 E > 29fJ irradiated - measured
			7, Fig 2, Page 1225	Graph shows the bending fracture strength and strain as a function of apparent density
Compressive Fracture Strain	0.165 ± 0.095 (X) 3.72 (Y) 0.710 ± 0.114 (Z)	%	7, Table 3, Page 1225	unirradiated - measured
	0.156 ± 0.057 (X) 0.111 ± 0.047 (Z)	%	7, Table 3, Page 1225	2 x 10^{25} n/m^2 E > 29fJ irradiated - measured
Compressive Strength	280	MPa	7, Table 1, Page 1224	II unirradiated - typical properties
	22	MPa	7, Table 1, Page 1224	⊥ unirradiated - typical properties
	59.8 ± 6.8 (X) 76.7 ± 14.0 (Y) 59.6 ± 6.7 (Z)	MPa	7, Table 3, Page 1225	unirradiated - measured
	55.9 ± 3.1 (X) 51.0 ± 7.3 (Z)	MPa	7, Table 3, Page 1225	2 x 10^{25} n/m^2 E > 29fJ irradiated - measured
CTE	-0.9	10^{-6}/K	7, Table 1, Page 1224	II unirradiated - typical properties
	8.3	10^{-6}/K	7, Table 1, Page 1224	⊥ unirradiated - typical properties
Density	1.83	g/cm^3	7, Table 1, Page 1224	⊥ unirradiated - typical properties
Length Changes	-2.11	l/l_o (%)	7, Table 2, Page 1224	caused by irradiation 2 x 10^{25} n/m^2 E > 29fJ
Volume Changes	-0.97	V/V_o (%)	7, Table 2, Page 1224	caused by irradiation 2 x 10^{25} n/m^2 E > 29fJ
Tensile Strength	>400	MPa	7, Table 1, Page 1224	II unirradiated - typical properties
	3	MPa	7, Table 1, Page 1224	⊥ unirradiated - typical properties
Thermal Conductivity	360 - 460	MPa	7, Table 1, Page 1224	II unirradiated - typical properties
	30-50	MPa	7, Table 1, Page 1224	⊥ unirradiated - typical properties
Young's Modulus	73 - 79	GPa	7, Table 1, Page 1224	II unirradiated - typical properties
	1.6 - 1.9	GPa	7, Table 1, Page 1224	⊥ unirradiated - typical properties

Mechanical Property	Value	Units	Reference	Notes
	74.0 (X) 87.6 (Z)	GPa	7, Table 3, Page 1225	unirradiated - measured
	98.0 (X) 87.2 (Z)	GPa	7, Table 3, Page 1225	2 x 10^{25} n/m^2 E > 29fJ irradiated - measured
			7, Fig 1, Page 1225	Graph shows Young's moduli as a function of apparent density

A16 PCC-1S

Mechanical Property	Value	Units	Reference	Notes
Ash Content	<20	ppm	8, Table 1 (b), Page 1127	unirradiated - makers data
Bending Strength	79.5	MPa	8, Table 1 (b), Page 1127	II unirradiated - makers data
	24.8	MPa	8, Table 1 (b), Page 1127	⊥ unirradiated - makers data
	79.5	MPa	8, Table 3 (b), Page 1129	II unirradiated experimental results - mean values
Bulk Density	1.86	g/cm^3	8, Table 1 (b), Page 1127	unirradiated - makers data
	1.89	g/cm^3	8, Table 3 (b), Page 1129	unirradiated experimental reaults - mean values
Compressive Strength	77.0	MPa	8, Table 1 (b), Page 1127	II unirradiated - makers data
	69.3	MPa	8, Table 1 (b), Page 1127	⊥ unirradiated - makers data
Electric Resistivity	425	μΩcm	8, Table 1 (b), Page 1127	II unirradiated - makers data
	778	μΩcm	8, Table 1 (b), Page 1127	⊥ unirradiated - makers data
Shore Hardness	32		8, Table 1 (b), Page 1127	II unirradiated - makers data
	25		8, Table 1 (b), Page 1127	⊥ unirradiated - makers data
Specific Heat	0.73	J/gK	8, Table 1 (b), Page 1127	II unirradiated - makers data
Thermal Conductivity	223	W/mK	8, Table 1 (b), Page 1127	II unirradiated - makers data * adjusted from table
	128	W/mK	8, Table 1 (b), Page 1127	⊥ unirradiated - makers data * adjusted from table
Thermal Expansivity	0.6	10^{-6}/K	8, Table 1 (b), Page 1127	⊥ unirradiated - makers data
	7.1	10^{-6}/K	8, Table 1 (b), Page 1127	II unirradiated - makers data
Thermal Shock Fracture Toughness	135	W/$mm^{1/2}$	8, Table 3 (b), Page 1129	II unirradiated experimental results - mean values
	95.4	W/$mm^{1/2}$	8, Table 3 (b), Page 1129	⊥ unirradiated experimental results - mean values
			8, Fig 4 (a), Page 1128	Graph shows the thermal shock fracture toughnesses of tested materials

Mechanical Property	Value	Units	Reference	Notes
Thermal Shock Resistance	>191	W/mm	8, Table 3 (b), Page 1129	II unirradiated experimental results - mean values
	30.9	W/mm	8, Table 3 (b), Page 1129	⊥ unirradiated experimental results - mean values
			8, Fig 4 (b), Page 1128	Graph shows the thermal shock resistances of tested materials
Youngs Modulus	36.3	GPa	8, Table 1 (b), Page 1127	II unirradiated - makers data
	5.9	GPa	8, Table 1 (b), Page 1127	⊥ unirradiated - makers data
	35.7	GPa	8, Table 3 (b), Page 1129	II unirradiated experimental results - mean values

A17 RFC

Mechanical Property	Value	Units	Reference	Notes
Diameter Change			10, Fig 2, Page 987	Graph shows the radiation induced diameter changes in RFC (2.44 x 10^{25} n/m^2, E > 50 keV, 1.6 dpa or 7.28 x 10^{25} n/m^2, E > 50keV, 4.7dpa)
Diameter Change			11, Fig 2, Page 1270	Graph shows the radiation induced diameter changes in RFC (2.44 x 10^{25} n/m^2, E > 50 keV, 1.6 dpa or 7.28 x 10^{25} n/m^2, E > 50keV, 4.7dpa)
Dimensional Changes			12, Fig 3, Page 2431	Graph shows the neutron irradiation induced dimensional changes - irradiated at 600°C
Fractional Change in Strength	1.00		11, Table 2, Page 1276	Unirradiated
	1.36		11, Table 2, Page 1276	Irradiated at a fluence of 0.9 DPA E > 50keV
	1.85		11, Table 2, Page 1276	Irradiated at a fluence of 2.67 DPA E > 50keV
Fracture Strength	30.8 ± 2.9	MPa	11, Table 2, Page 1276	Unirradiated
	41.9	MPa	11, Table 2, Page 1276	Irradiated at a fluence of 0.9 DPA E > 50keV
	57.0	MPa	11, Table 2, Page 1276	Irradiated at a fluence of 2.67 DPA E > 50keV
Length Change			10, Fig 1, Page 987	Graph shows the radiation induced length changes in RFC (2.44 x 10^{25} n/m2, E > 50 keV, 1.6 dpa or 7.28 x 10^{25} n/m^2, E > 50keV, 4.7dpa)
Length Change			11, Fig 1, Page 1270	Graph shows the radiation induced length changes in RFC (2.44 x 10^{25} n/m2, E > 50 keV, 1.6 dpa or 7.28 x 10^{25} n/m^2, E > 50keV, 4.7dpa)
Strength			11, Fig 8, Page 1277	Graph shows the effect of neutron irradiation on the strength of RFC (2.44 x 10^{25} n/m^2, E > 50 keV, 1.6 dpa or 7.28 x 10^{25} n/m^2, E > 50keV, 4.7dpa)
Volume Change			10, Fig 3, Page 987	Graph shows the radiation induced volume changes in RFC (2.44 x 10^{25} n/m^2, E > 50 keV, 1.6 dpa or 7.28 x 10^{25} n/m^2, E > 50keV, 4.7dpa)

Mechanical Property	Value	Units	Reference	Notes
Volume Change			11, Fig 4, Page 1273	Graph shows the radiation induced volume changes in RFC (2.44 x 10^{25} n/m^2, E > 50 keV, 1.6 dpa or 7.28 x 10^{25} n/m^2, E > 50keV, 4.7dpa)

A18 UFC

Mechanical Property	Value	Units	Reference	Notes
Diameter Change			10, Fig 2, Page 987	Graph shows the radiation induced diameter changes in UFC (2.44 x 10^{25} n/m^2, E > 50 keV, 1.6 dpa or 7.28 x 10^{25} n/m^2, E > 50keV, 4.7dpa)
Diameter Change			11, Fig 2, Page 1270	Graph shows the radiation induced diameter changes in UFC (2.44 x 1025 n/m2, E > 50 keV, 1.6 dpa or 7.28 x 10^{25} n/m^2, E > 50keV, 4.7dpa)
Dimensional Changes			12, Fig 3, Page 2431	Graph shows the neutron irradiation induced dimensional changes - irradiated at 600°C
Fractional Change in Strength	1.00		11, Table 2, Page 1276	Unirradiated
	1.55		11, Table 2, Page 1276	Irradiated at a fluence of 2.81 DPA
Fracture Strength	9.43 ± 0.59	MPa	11, Table 2, Page 1276	Unirradiated
	14.6	MPa	11, Table 2, Page 1276	Irradiated at a fluence of 2.81 DPA
Length Change			10, Fig 1, Page 987	Graph shows the radiation induced length changes in UFC (2.44 x 10^{25} n/m^2, E > 50 keV, 1.6 dpa or 7.28 x 10^{25} n/m^2, E > 50keV, 4.7dpa)
Length Change			11, Fig 1, Page 1270	Graph shows the radiation induced length changes in UFC (2.44 x 10^{25} n/m^2, E > 50 keV, 1.6 dpa or 7.28 x 10^{25} n/m^2, E > 50keV, 4.7dpa)
Strength			11, Fig 8, Page 1277	Graph shows the effect of neutron irradiation on the strength of UFC (2.44 x 10^{25} n/m^2, E > 50 keV, 1.6 dpa or 7.28 x 10^{25} n/m^2, E > 50keV, 4.7dpa)
Volume Change			10, Fig 3, Page 987	Graph shows the radiation induced volume changes in UFC (2.44 x 10^{25} n/m^2, E > 50 keV, 1.6 dpa or 7.28 x 10^{25} n/m^2, E > 50keV, 4.7dpa)
Volume Change			11, Fig 4, Page 1273	Graph shows the radiation induced volume changes in UFC (2.44 x 10^{25} n/m^2, E > 50 keV, 1.6 dpa or 7.28 x 10^{25} n/m^2, E > 50keV, 4.7dpa)

Appendix B: Incoloy 800H Information Table (Helium Tested)

Mechanical Property	Value	Units	Reference	Notes
Carbon Change			21, Fig 2, Page L12	Graph shows dilation vs. carbon change
Carbon Increase			20, Fig 5, Page J19	Graph shows the rates of carbon increase in Incoloy 800H as a result if exposure to helium environments
Creep-Fatigue			22, Fig 9, Page U11	Graph shows a creep fatigue interaction diagram
Creep Rupture Strength			17, Fig 4, Page 254	Graph shows the creep rupture strength of materials under consideration for advanced HTRs
Creep Rupture Strength			18, Fig 3, Page 20	Graph shows the influence of carbon, titanium and aluminium on creep rupture strength of Alloy 800
Fatigue Behaviour			17, Fig 8, Page 22	Graph shows the low cycle fatigue behvoiur of alloy 800
Fatigue Behaviour			22, Fig 3, Page U9	Graph shows the influence of temperature and environment on the fatigue behaviour
Fatigue Design Curve			22, Fig 10, Page U12	Graph shows the suggested fatigue design curve for elastic analysis and Incoloy 800H at 850°C
Hold Time Tests			22, Fig 7, Page U11	Graph shows the results of hold time tests at 750°C
			22, Fig 8, Page U11	Graph shows the results of hold time tests at 850°C
Impact Energy			17, Fig 11, Page 258	Graph shows the impact energy for HTR alloys after isothermal exposure at 900°C
Strain Limit			18, Fig 6, Page 21	Graph shows the mean values for the 1% strain limit
Stress Rupture Strength			18, Fig 5, Page 21	Graph shows the stress rupture strength
Stress Rupture Strength			19, Fig 18, Page 90	Stress rupture test results before and after reactor irradiation
Stress/Strain			18, Fig 7, Page 21	Graph shows an example of isochronous stress strain curves
Tensile Stress			17, Fig 9, Page 254	Graph shows the max. tensile stress vs. strain rate in LCF tests
Dilation Experiments			Ref 21	

Appendix C: Carbon/Carbon Composite Documents

Ref 3: **Neutron irradiation effect on the thermal conductivity and dimensional change of graphite materials**

This document contains the results of tests to determine the effect on the thermal conductivity of neutron irradiation for various materials including a carbon-carbon composite material (CX-2002U). The dimensional changes were also investigated.

Ref 4: **Thermal diffusivity of neutron irradiated carbon-carbon composites**

The thermal diffusivity of two kinds of carbon-carbon composites (A05 and 190G) is investigated following neutron irradiation in the JMTR. The changes in thermal conductivity related to thermal diffusivity are also discussed in this document.

Ref 5: **The characteristics of cracks and voids in two dimensional carbon-carbon composites**

This document contains examination of sections of 2D carbon fibre reinforced carbons using optical and scanning electron microscopy. The voids in the materials are classified according to their position, size and orientation into 4 groups; co-planar, bundle and inter-fibre cracks and inter-fibre pores.

Ref 6: **Thermal conductivity changes in graphites and carbon/carbon fibre materials induced by low neutron damages**

Various materials including some carbon/carbon fibre composites were irradiated in the Pool Side Facility (PSF) of the High Flux Reactor (HFR Petten). This document investigates the effect of the irradiation on the thermal conductivities using the Laser Flash Method and the Kohlrausch Method.

Ref 7: **Mechanical properties of neutron irradiated carbon-carbon composites for plasma facing components**

This document contains the irradiation effects on the mechanical properties of three kinds of carbon-carbon composites (CX-2002U, MFC-1 and CC-312). The graphite IG 110 was also irradiated as a reference material. The properties measured were dimensional changes, Young's moduli, bending and compressive strengths.

Ref 8: **Evaluation of Performance for Plasma Disruption and Neutron Irradiation for Graphites and C/C Composites as First Wall Components for Fusion Reactor Devices** *(in Japanese, abstract and data in English)*

This document contains investigations into the thermal shock resistance and fracture toughness of several kinds of graphites and C/C composites by means of arc discharge heating for disk specimens. The mechanical and fracture mechanics are also measured. Following neutron irradiation in the JMTR, the degradations in the thermal shock resistance and fracture toughness and the changes of mechanical and fracture mechanics properties are measured.

Ref 9: **Effect of Irradiation on Mechanical Properties of Carbon Composite Materials** *(in Japanese, abstract and data in English)*

In this document three types of C/C composite are investigated (CC-312, CX2002-U and MCI). The relationship between the change of mechanical properties due to irradiation and the constitution of the C/C composite materials was evaluated.

Ref 10: **Radiation Damage in Carbon/Carbon Composites**

This document evaluates irradiation induced dimensional changes in 1D, 2D and 3D carbon-carbon composites (A05, UFC, RFC, 225 and 222) for fluences up to 4.7 dpa at an irradiation temperature of 600°C. H-451 is used as a reference material**.**

Ref 11: **The Effect of Neutron Irradiation on the Structure and Properties of Carbon-Carbon Composite Materials**

This document is an updated version of Reference 8. Apart from radiation induced dimensional changes, also measured are Fracture Strength, the fractional change in strength and the Thermal Conductivity.

Ref 12: **Irradiation induced structure and property changes in Tokamak plasma facing C/C composites**

This document contains data on two irradiated C/C composites. Radiation induced dimensional changes are discussed in terms of their architecture, fibre type and graphitisation temperature. Thermal Conductivity changes are also reported. The materials tested were UFC, RFC, 223 and 222 and a peak damage dose of 4.7 dpa at 600°C was attained.

Ref 13: **Burst Tests to Measure the Tangential Strength of CFC Tubes**

In this document, Carbon Fibre Reinforced Composites (CFC) are considered as graphite/metal substitute material for certain structural components in modern HTR design. The C/C material tested was Sigri CC 2001G. The document contains information on the mechanical properties of this material.

Ref 14: **Development of Carbon/Carbon Composite Control Rod for HTTR (II) - concept, specifications and mechanical test of materials**

This document contains data on the room temperature properties of C/C composites, AC 250 (UD), AC 250 (2D) and CX-270. The properties investigated are Tensile Strength, 3-Point Bending Strength, Compressive Strength, Shear Strength, Young's Modulus, Thermal Conductivity, Thermal Expansion Coefficient, Specific Heat, Density and Electrical Resistivity. The results are believed to indicate the mechanical integrity of the control rod structure of the HTTR.

Ref 15 **High Temperature Carbon irradiation Issues for the Sombrero ICF Reactor**

In order to assess the feasibility of carbon materials for the first wall of the Sombrero KrF laser-driven ICF fusion reactor, published experimental results relating to mechanical and thermal properties of graphites and carbon-fibre composites (CFCs) under neutron irradiation and high heat loads are reviewed. Results are compared with published design requirements considering erosion, radiation induced swelling and Tritium retention. The results indicate the urgency for high temperature neutron irradiated tests of CFCs.

Ref 16 The fatigue strength of graphite and carbon materials for HTTR core components

Room temperature fatigue tests were carried out on graphite and carbon materials to be used for the core region of the HTTR. Tests were also carried out on IG-110 graphite at 980^{o}C to clarify the effect of temperature on fatigue strength. The fatigue decreased with R value. Design fatigue curves were obtained on PGX and ASR-ORB. Fatigue strength of IG-110 at 980^{o}C appeared to be almost the same as that at room temperature, if the applied stress was normalised to the mean tensile strength at room temperature in a vacuum.

Appendix D: Alloy 800H Documents – (Helium Tested)

Ref 17: Evaluation of Alloys for Advanced High-Temperature Reactor Systems

For the heat exchanging components of a HTR, high temperature creep resistant alloys are required for long operation times. The availability of creep resistant material for the temperature range 800 – 1000°C is an important aspect for the feasibility of advanced HTR systems. Alloy 800H is qualified up to 750°C for the steam cycle HTR. The qualification is based on creep behaviour, fatigue properties, structural stability and corrosion resistance. This document presents a selection of typical results.

Ref 18: Service Conditions and Relevant Properties of HTGR Materials

Special materials requirements have arisen for HTGRs because of the high temperatures, the properties of the coolant and neutron irradiation in regions adjacent to the core. The operational conditions of components such as steam generators, helium/helium heat exchangers, steam reformers and control and shut down rods are presented in this document. Data for the most important material properties for components layout is described.

Ref 19: Current Status of Studies on High Temperature Metallic Material for HTGR Application in JAERI

Section 4 of this document is entitled "Cladding Material for neutron absorber rods (Alloy 800H)". The cladding material of the neutron absorber rods is subjected to irradiation induced loss of ductility at high temperatures. This is due to helium generated through transmutations by thermal neutrons. Iron base alloys are generally superior to nickel rich alloys in both post irradiation tensile and creep properties.

Fig 18: Graph "Stress Rupture Results on Hastelloy X and Alloy 800 before and after irradiation"

Alloy 800H was selected as one of the currently most realistic candidate materials for the cladding material for the neutron absorber rods of the HTTR. Post irradiation creep tests are being carried out using new test machines designed for testing in an inert environment. Final selection is subject to the safety reviewing of the authorities particularly in terms of the service temperature in the design.

Ref 20: Interaction of Metals with Primary Coolant Impurities: Comparison of Steam-Cycle and Advanced HTGRs

The carburisation behaviour of various materials including Incoloy 800H in helium containing various amounts of H_2, CO, CH_4, H_2O and CO_2 is presented in this document. Corrosion tests were conducted in the temperature range 649 to 1000°C exposure times up to 10,000 h. Thermodynamic analyses were also performed. The results suggested that controlling the oxygen potential of the service environment can be an effective means of reducing the carburisation of alloys.

Ref 21: Relationship Between Carburisation and Zero-Applied-Stress Creep Dilation in Alloy 800H and Hastelloy X

Typical candidate alloys can carburise when exposed to simulated service environments. The carbon concentration gradients so formed give rise to internal stresses which could cause dilation. Studies performed with Hastelloy X and Alloy 800 H showed that dilations of up to almost 1% can occur at 1000°C when carbon pickup is high. Dilation was normally observed only when the carbon increase was >1000 $\mu g/cm^2$ and ceased when the diffusing carbon reached the centre of the specimen.

Ref 22: Fatigue and Creep Fatigue Behaviour of High Temperature Alloys for HTR Application

The development of High Temperature Gas-Cooled Reactors requires the evaluation of the fatigue behaviour of those alloys which have been taken into account for possible use as structural materials. This document contains the results of fatigue tests of 6 wrought alloys including Incoloy 800H at 850°C.

Appendix E: List of Alloy 800H Documents

Ref No	Authors	Title	Source	Year	Materials	Tests/Data	Temperature	Graphs	Tables	Environment
17	H Nickel, F. Schubert and H. Schuster	Evaluation of Alloys for Advanced High-Temperature Reactor Systems	0029-5493/84 Elsevier Science Publishers B.V. (North Holland Physics Publishing Division) P251-P 265.	1983	INCOLOY 800 H (X 10 NiCrAlTi 32 20) HASTELLOY X (NiCr 22 Fe 18 Mo) INCONEL 617 (NiCr 22 Co 12 Mo) NIMONIC 80 A ALLOY 713 LC TZM SSS113 MA	Creep behaviour behaviour during Short Term Load Fatigue behaviour Properties after Long-Time Annealing Corrosion Caused by the Operating Gases	600-950°C	Material Tempertures and Design Codes Creep Rupture Strength Creep Properties Comparison of Measured Creep Rates with Calculated Creep Rates Stress/Strain Curves LCF Results Max Tensile Stress Time-Temperture Precipitation Impact Energy for HTR Alloys Creep Rupture Properties Influence of Structure on Fracture Strain Linear Damage Fatigue	Nominal Compositions of High Temperture Alloys Gas Compositions in Advanced HTRs	Air Helium $H_2 + CO + CO_2$
18	K. Spradek, H. P. Degischer and H. Lahodny	Correlation Between Microstructure and the Creep Behaviour at High Temperature of Alloy 800 H	High Temperature Metallic Materials for Gas-Cooled Reactors Proceedings of a Specialists Meeting Organised by the International Atomic Energy Agency and Held in Cracow, 20-23 June 1988	1988	Alloy 800 H	Creep Testing Proceedure Microstructural Examinations Identification of Creep Stages Microstructural Interpretation Creep Stages Map	800 ± 4°C	Time-Temperature-Precipitation Diagram of Alloy 800 H Stress Curves for Alloy 800 H Schematic Representation of the Creep Stages Observed Alloy 800 H Comparison of the Strain-Rate Curves for Alloy 800 H Curves for samples tested with 45 MPa at 800°C Comparison of Creep-Rate Curves for Differently Predeformed Alloy 800 H Creep Stages Map for Alloy 800 H tested at 800°C	None	Pressure
19	H. Tsuji, H. Nakajima and T. Kondo	Current Status of Studies on High Temperture Metallic Materials for HTGR Applications in JAERI	High Temperature Metallic Materials for Gas-Cooled Reactors Proceedings of a Specialists Meeting Organised by the International Atomic Energy Agency and Held in Cracow, 20-23 June 1988	1988	Hastelloy XR Ni-Cr-W Superalloys Alloy 800H	Creep Fatigue Corrosion Thermal Aging Long-term Target Alloys for Structural Components Cladding Material for Neutron Absorber Rods	<1000°C	Creep-Rupture Data for Hastelloy XR Comparison of Creep-Rupture Data Relation Between Total Boron Content & Creep Rupture Strength Effect of Boron Content on Number of Cracks per one Cross Section Effect of Boron Content on Time to Rupture for Hastelloy XR Comparison of Creep Rupture Times of Hastelloy XR & XR-II Relation Between Total Strain Range & Fatigue Life Effect of Hold Time on Low-Cycle Fatigue Life Hold Time Dependence of the Fatigue Life in Tensile Hold-Time Experiments Total Strain Ranges vs Number of Cycles to Failure Relation between Normalized Strain Range vs Cycles to Failure Fatigue Life as a Function of Test Temperature & Total Strain Range Depth of Cr Depleted Zone vs Exposure Time Oxidation Kinetics of Hastelloy XR-II vs Hastellloy XR Room Temperature Impact Value of Hastelloy XR after Heating Effect of Ni-Cr-W Composition on Creep Rupture Strength Effect of Ni-Cr-W Composition on Corrosion Resistance	High Temperture Alloys for HTGR Applications Impurity Levels in JAERI-type B Helium Impurity Composition in Helium Environments	JAERI-type B Helium Air

Ref No	Authors	Title	Source	Year	Materials	Tests/Data	Temperature	Graphs	Tables	Environment
								Stress Rupture Test Results on Hastelloy X and Alloy 800		
20	W. R. Johnson and G. Y. Lai	Interaction of Metals with Primary Coolant Impurities: Comparison of Steam-Cycle and Advanced HTGRs	Specialists' Meeting on High Temperture Metallic Materials for Application in Gas-Cooled Reactors Vienna, Austria 4-6 May 1981	1981	Incoloy 800H Inconel 617 Hastelloy X	Corrosion Tests Environmental Tests	Various	Mass of Carbon Increase Rates of Carbon Increase Calculated Carbon Activities Equilibrium Oxygen Partial Pressure for Various Metallic Oxides Stability Diagram for the Cr-O-C system	Exposure Conditions for Alloys under Investigation Characteristics of Alloys under Investigation	Varying Helium Atmospheres
21	H. Inouye and P. L. Rittenhouse	Relationship Between Carburization and Zero-Applied-Stress Creep Dilation in Alloy 800H and Hastelloy X	Specialists' Meeting on High Temperture Metallic Materials for Application in Gas-Cooled Reactors Vienna, Austria 4-6 May 1981	1981	Alloy 800H Hastelloy X	Dilation Measurements	1000°C	Dilation vs Carbon Change Dilation vs Exposure Time	Gas Composition and Exposure Times for Dilation Experiments Summary of Dilation Experiments	HTGR Helium
22	H. P. Meurer, H. Breitling and E. D. Grosser	Fatigue and Creep Fatigue Behaviour of High Temperture Alloys for HTR Application	Specialists' Meeting on High Temperture Metallic Materials for Application in Gas-Cooled Reactors Vienna, Austria 4-6 May 1981	1981	Incoloy 800H Incoloy 8002 Hastelloy X Hastelloy S Nimonic 86 Inconel 617	Comparative Tests in air at 850°C Influence of Temperature and Environment Influence of Hold Times Inelastic Analysis Elastic Analysis	750°C 850°C 950°C	Influence of Temperature and Environment on Fatigue Behaviour Results of Hold Time Tests Creep-Fatigue Interaction Diagram Suggested Fatigue Design Curve for Elastic Analysis	Alloys Tested, Chemical Composition, Product Form Composition of Impurities in the Helium Atmosphere	Air Impure Helium
23	L.W. Graham	Corrosion of Metallic Materials in HTR-Helium Environments	Journal of Nuclear Materials 171 (1990) North -Holland P76-P83	1990	Alloy 800H Inconel 617 Hastelloy X 713LC IN-100	Effects due to: Decarburisation Carbon Deposition/Carburisation Loss of Section due to Internal Oxidation Spalling of Surface Scales	623-873 K 873-1073 K 1073-1273 K	Dependence of Microclimate Temperature T_A	Ranges of Impurity Levels Expected in HTR Chemical Compositions Scatter of Carburisation	HTR Helium with Impurities
24	P.J. Maziasz, R.W. Swideman, J.P. Montague, M. Fitzpatrick, P.F. Browning, J.F Grubb, R.C. Klug and R.A. Painter	Stainless Steel Foil with Improved Creep-Resistance for Use in Primary Surface Recuperators for Gas Turbine Engines	Conference Proceeding from Materials Solutions 1998 P70-P78	1998	type 316 SS 17-14 CuMo SS TP347H SS HT-UPS mod.316 310HCbN NF709 alloy 800H HT-UPS mod. 800H type 347 SS (heat cert. 41271) type 347 SS (heat AL 848691)	Creep Tests	732°C	Creep Strain vs Time Curves Design Stress for Superheater Tubing	Compositions of Various Austenitic Stainless Steels and Alloys	Air
25	D. H. Yates, P. Ganesan and G. D. Smith	Recent Advances in the Enhancement of Inconel Alloy 617 Properties to Meet the Needs of the Land Based Gas Turbine Industry	Advanced Materials and Coatings for Combustion Turbines Proceedings of ASM 1993 Materials Congress pp 89-97	1993	INCONEL Alloy 617 INCONEL Alloy 230 INCONEL Alloy HX INCONEL Alloy 188 INCONEL Alloy 86 INCONEL Alloy S INCONEL Alloy 214 INCONEL Alloy 625 INCONEL Alloy C-276 INCONEL Alloy 601 INCONEL Alloy 600 INCONEL Alloy 800 INCONEL Alloy 330 INCONEL Alloy DS INCONEL Alloy 309	Oxidation Tests Oxygen-Sulpher Dioxide Tests Carburisation Tests Burner Rig Tests Metallurgical Stability Weldability and Formability LCF Considerations Fabrication Considerations	Various	Creep strength of solution-annealed INCONEL alloy 617 Mass change vs exposure time in air + 5% water vapour Mass change vs exposure time in air + 20% water vapour Mass change in cyclic oxidation test vs exposure time Mass Change vs exposure time Effect grain size on the tension-tension axial stress controlled LCF properties Effect of temperature on the tension-tension axial stress Effect of cold work and susequent annealing temperature	Nominal compositions of alloys in this study Mass change in cyclic oxidation test at 1093°C Metal loss and depth of minimum attack data Mechanical properties after exposure to elevated temperature Room Temperature tensile properties Effect of grain size on the tension-tension axial stress controlled LCF Charpy impact impact results	Air Air + water vapour Oxygen + sulphur dioxide
26	V. Guttmann and M. Schutze	Interactions of Corrosion and Mechanical Properties	High Temperature Alloys for gas turbines	1986	Alloy 800 Alloy 800 H	Creep Testing Procedures Oxide Failure Properties	>700°C	Oxide Failure Mode Map Scale Failure Diagram for Alloy 800	None	Various

Ref No	Authors	Title	Source	Year	Materials	Tests/Data	Temperature	Graphs	Tables	Environment
			and other applications 1986. Proceedings of a Conference held in Liege, Belgium, 6-9 October 1986 vol 1 pp 293-326		14 MoV 6 3 Ni 270 Inconel Alloy X-750 HK40 IN738 LC IN751 IN939 IN100 RA 333 Haynes 188 HP 40 Nb	Effect of Stress on Corrosion Creep (Tensile-) Behaviour in Oxidising Atmospheres Creep Behaviour in Carburising Atmospheres Creep Behaviour in Sulphidising Atmospheres Gas Turbine Conditions Coal Conversion Process		Enhancement of Internal Oxidation of Alloy 800H Rupture Lifetime of 14 MoV 6 3 Steel for Various Temps in Air & Helium Creep Ductility of 14 MoV 6 3 Steel in Air & Helium Tensile Ductility of Ni 270 at 800°C in Argon Influence of Test Piece Geometry in Creep for Inconel Alloy X-750 Creep Curves for Ni 270 Creep Rupture Strength for HK40 1% Creep Strength for HK40 Elongation to Fracture vs Time to Rupture for HK40 Oxygen-Sulphur-Temperature Diagram Phase Stability in (Fe, Ni, Co, Mn)-S-O systems at 870°C Creep Curves for IN 738 LC for Different Deposits and for Air Rupture Lifetime of IN 751 for 90% Na_2SO_4/10% NaCl Coatings & in Air Creep Curves for Seasalt Coated IN 939 Rupture Lifetime for IN 939 in Air and SO_2/SO_3/Air Mixture Relative Rupture Life Degradation in Sulphate/Chloride Salt at 704°C Rupture Lifetime for IN 100 in Different Gases Rupture Lifetime for IN 738 LC in Different Gases Rupture Lifetime in S-O-C Gas and in Air at 69 Bar Rupture Li		
27	E. Bodmann, H. Diehl, I. Blume-Firla and H Demus	Service Conditions and Relevant Properties of HTGR Materials	High Temperature Metallic Materials for Gas-Cooled Reactors Proceedings of a Specialists Meeting Organised by the International Atomic Energy Agency and Held in Cracow, 20-23 June 1988	1988	Alloy 800 IN617 Hastelloy X	Mechanical Properties Creep Rupture Tests Stress Rupture Tests Coating for Protection Irradiation Stability of Control & Shutdown Rod Material	Various	Influence of Carbon, Titanium and Aluminium on Creep Rupture Strength Isothermal Creep Rupture Curves with Scatter Mean Values of 1% Strain Limit for Alloy 800 HT Example of Isochronous Stress Strain Curves for Alloy 800 HT LCF behaviour of Alloy 800 Solution Treated at 1100-1200°C Creep Rupture Strength Determined in Short Term Tests Rupture Strain of Steel 1.4981 after Irradiation	Service Conditions of a Steam Generator Service Conditions of He/He Heat Exchanger and Steam Reformer Service Condtions of Control Rods Standard Materials for HT Service Material Data Bank Alloy 800 Tests on Structural Stability Experiments to Test Coatings Against Friction and Wear Comparison of the 3 Alloy 800 Variations for HTR Application Contents of Material Data Sheet Alloy 800: Standard Preparation by DIN	Helium Air
28	W. J. Quadakkers, and H. Schuster	Corrosion behaviour of High Temperature Alloys in the Cooling Gas of High Temperature Reactors	High Temperature Metallic Materials for Gas-Cooled Reactors Proceedings of a Specialists Meeting Organised by the International Atomic Energy Agency and Held in Cracow, 20-23 June 1988	1988	Inconel 617 Hastelloy X Nimonic 86 Alloy 800 H Thermon 4972	Gas Composition & Temp Dependence of Corrosion	850-950°C	Corrosion Areas in Modified Stability Diagram for Chromium Change in Carbon content of INCONEL 617 during exposure in "PNP helium" Scale of formation of INCONEL 617 Creep Curves for INCONEL 617 Influence of CO Partial Pressure on the change in Carbon Content Microstructure of INCONEL 617 after 1000h exposure at 950°C	None	HTGR Helium PNP Helium

Ref No	Authors	Title	Source	Year	Materials	Tests/Data	Temperature	Graphs	Tables	Environment
								Corrosion Kinetics of INCONEL 617 at 950°C		
29	M. Rodig, M. Pfaffelhuber, F. Schubert, E. Bodmann and H. Nickel	Creep and Fatigue Crack Growth in Tubes of HTR Components	High Temperature Metallic Materials for Gas-Cooled Reactors Proceedings of a Specialists Meeting Organised by the International Atomic Energy Agency and Held in Cracow, 20-23 June 1988	1988	Alloy 800	Fatigue Crack Growth Experiments	550°C	Calculated Stress Intensity Factors Progression of Crack Depth in a FCG Experiment Crack Growth Rate Progression of Crack Propagation in a Creep Crack Growth Rate Crack Growth Velocity	None	Pressure
30	W. Pelz, W. Schendler and H. Weber	Comparison of Mechanical and Corrosion Behaviour of Alloy 800H and the New Alloy AC66	High Temperature Metallic Materials for Gas-Cooled Reactors Proceedings of a Specialists Meeting Organised by the International Atomic Energy Agency and Held in Cracow, 20-23 June 1988	1988	Alloy 800H Alloy AC66	Corrosion Behaviour Mechanical Behaviour Creep-Rupture Strength Cyclic Strain Tests	Various	Weight Loss Due to Corrosion on Alloys Chromium Content at the Steel/Scale Boundary Region Weight Change at Thermal Cycles Internal Oxidation as a Function of Aluminium Content Relationships Between Weight Loss, Internal Oxidation and Time Stability Diagram for some Alloying Elements Creep Rupture Strength Number of Cycles to Failure Comparison of Alloys in Process Gas Relationship Between Reduction in Wall Thickness & Time	Chemical Composition of AC 66 compared with Incoloy 800H	Air Process Gas
31	D. Schuhmacher and U. Bruch	Materials Behaviour in Methane Reforming Gas	Specialists' Meeting on High Temperture Metallic Materials for Application in Gas-Cooled Reactors Vienna, Austria 4-6 May 1981	1981	INC 800H INC 802 Hastelloy X Nimonic 86 Inconel 617 IN519 Manaurite 36 X	Corrosion Behaviour Creep Rupture Properties Morphology of Oxide Scales	800°C 950°C	Thermal Gravimetric Analysis of Corrosion in Steam Reformer Atmosphere Corrosive Wear in Steam Reformer Atmosphere Corrosive Wear of High Temperature Alloys in Steam Reformer Atmosphere Internal Oxidation and Carbon Depletion Creep Curves Creep Rupture Strength	Chemical Composition of High Temp Alloys	H_2O/CH_4
32	W. J. Quadakkers	Corrosion of High Temperature Alloys in the Primary Circuit Helium of High Temperature Gas Cooled Reactors. - Part 2: Experimental Results	Werkstoffe und Korrosion 36, 335-347 (1985)	1985	INCONEL 617 NIMONIC 86 HASTELLOY X INCOLOY 800 H NSC-1 IRW-I IRW-II Ni-25 Cr	Construction of a stability diagram, used to correlate corrosion results		Change in the carbon monoxide pressure during heating of alloy NiCr22Co12Mo Measured P_{CO} for different alloys compared with calculated values Calculated chromium profiles for different exposure times Calculated relation between chromium activity and chromium concentration Stability diagrams for alloy NiCr22Co12Mo at 900°C and 950°C Change in carbon content of NiCr22Co12Mo & NiCr25Mo after 300h exposure Influence of water level on carbon transfer and scale formation Kinetics of carbon transfer of NiCr22Co12Mo & NiCr22Fe18Mo Carbon uptake and scale formation of NiCr22Co12Mo and NiCr22Fe18Mo Oxidation rate constants K_n of NiCr22Co12Mo	Compositions of the alloys used in the experiments Principle gas compositions used in the experiments Calculated valued of P_{O2} and a_c for the PNP reference alloys Change in gas composition during exposure of NiCr22 Co12Mo in He-H2/Ch4/H2O	

Ref No	Authors	Title	Source	Year	Materials	Tests/Data	Temperature	Graphs	Tables	Environment
								andNiCr22Fe18Mo Influence of titanium additions in NiCrW-alloys on time dependence C transfer		
33	J. Bressers, L. Remy and W. Hoffelner	Fatigue Dominated Damage Processes	High Temperature Alloys for gas turbines and other applications 1986. Proceedings of a Conference held in Liege, Belgium, 6-9 October 1986 vol 1 pp 441-468	1986	PM Astroloy Alloy 800 H Waspaloy Mar M 509 IN100 HIP + Forged Astroloy IN738 LC Hastelloy X IN800 H IN617 RA 333 A 286 IN718 IN901 IN939	Dislocation Substructures Microstructural Instabilities Localised damage on the scale of the microstructure Transgranular crack initiation Intergranular crack initiation Crack growth	Various	Deformation modes in PM Astroloy Dependence of the Cyclic Saturation Stress of Alloy 800H Number of Cycles for Microcrack Initiation N_i Oxidation Induced Frequency Effect on n^o of Cycles Initiating a Crack Transgranular to Intergranular Transition in Mode of Crack Initiating Variation of Life Fraction Ni/Nf spent initiating a 0.25mm deep crack Fatigue Crack Growth Rate of Physically Short Cracks Crack Opening Intensity Factor of Short Cracks Growth Rates of Deep Cracks in Fully Yielded Specimens of Mar-M509 Comparison of Short and Long Crack Growth Rates in PM Astroloy Fatigue Crack Growth Rates of Long Cracks for Various High Temp Alloys Effect of Test Temperature on Fatigue Crack Growth Rates Fatigue Crack Growth Rates of Long Cracks in f.g. & c.g. IN 901 The Effect of Test Temperature on the Threshold Value	None	Air Vacuum
34	H. J. Penkalla, F Schubert and H. Nickel	Multiaxial Creep of Tubes of Alloy 800 and Alloy 617 at High Temperature	High Temperature Metallic Materials for Gas-Cooled Reactors Proceedings of a Specialists Meeting Organized by the International Atomic Energy Agency and Held in Cracow, 20-23 June 1988	1988	Alloy 800 Alloy 617	Multiaxial Creep Data	950°C	Boundaries Between Different Behavior of Metallic Material Stationary Creep Rate of INCONEL 617 Dependent on the Uniaxial Stress Deviatoric Stresses and Times to Failure for a Heat Exchanger Tube Creep Damage in Tubes Under Internal Pressure & Tensile Load Comparison of Lifetimes of Steam Reformer & Heat Exchanger Tubes Redistribution of Strain Rates Under Different Loading Conditions Interaction Between the Constant Tensile Stress & Relaxing Tortional Shear Creep Strain of INCONEL 617 Increase of Axial Strain Rate of an INCONEL 617 IHX-Tube Relaxing Tortional Shear Stress Tortional Shear Strain in Dependence on Time Tortional Shear Strain and Axial Strain	Form of Specimens and Investigated Materials Loading Conditions	Air